aerospace

MDPI

Article

Iterative LMI-Based Plant–Controller Co-Design Using Explicit Model Following Control: A VTOL Application

Ethem Hakan Orhan * and Ozan Tekinalp

Aerospace Engineering, Middle East Technical University, Ankara 06800, Turkey; tekinalp@metu.edu.tr
* Correspondence: ethem.orhan@metu.edu.tr

Abstract

A plant–controller co-design methodology is proposed in which the reference model dynamics are parameterized and incorporated directly into the optimization rather than prescribed a priori. Within an Explicit Model Following (EMF) architecture, plant-design variables and reference-model parameters are optimized simultaneously with the controller gains, subject to prescribed stability, performance, and maneuverability constraints. The framework accommodates H_2, H_∞, and mixed H_2/H_∞ state-feedback synthesis and can be extended to multiple design points. The bilinearities arising from the coupled plant–controller–reference model optimization are addressed through a perturbation-based iterative procedure that decomposes the resulting Bilinear Matrix Inequality (BMI) problem into sequential convex Linear Matrix Inequality (LMI) subproblems. The proposed framework is demonstrated and validated through an integrated sizing and control-design problem for a representative quad-wing tilt-rotor Vertical Take-Off and Landing (VTOL) air vehicle, where aircraft-specific maneuverability and handling-quality requirements are incorporated as design constraints. Compared with the initial controller design obtained for fixed plant parameters, the final co-designed plant–controller configuration achieves a substantial improvement in closed-loop performance, with the maximum control demand reduced by approximately 70% in the directional control case. Further optimization of the reference-model parameters yields an additional 3–5% improvement in control effort metrics, indicating that the prescribed closed-loop dynamics can influence the overall co-design optimum while maintaining the required handling-quality constraints.

Keywords: integrated plant–controller design; co-design; linear matrix inequalities; explicit model following control; quad-wing aircraft; vertical takeoff and landing

Check for updates

Academic Editor: Bin Zhou

Received: 25 August 2026
Revised: 10 October 2026
Accepted: 11 October 2026
Published: 15 October 2026

Copyright: © 2026 by the authors. Licensee MDPI, Basel, Switzerland. This article is an open access article distributed under the terms and conditions of the Creative Commons Attribution (CC BY) license.

1. Introduction

Sequential design procedures remain widely used in aerospace engineering because of their simplicity and practical effectiveness. In a conventional design workflow, air-vehicle parameters are first selected or optimized according to objectives such as mass, aerodynamic efficiency, and structural constraints. The flight control system is subsequently designed for the resulting plant to satisfy prescribed stability, control, and maneuverability requirements. This separation, however, does not explicitly account for the coupling between vehicle dynamics and control-system performance and may therefore lead to conservative or suboptimal closed-loop designs. Integrated plant–controller design addresses this limitation by considering plant and controller parameters within a common optimization framework [1]. The concept has been referred to by various terms in the

literature, including co-design, integrated plant and control design, combined plant and control optimization, optimal redesign, and simultaneous design [2–4].

Two principal classes of solution strategies have been proposed for integrated plant–controller design. The first treats plant and controller variables simultaneously within a single optimization problem, whereas the second alternates between controller synthesis and plant-parameter optimization [5,6]. Even when the state-space matrices depend affinely on the plant-design parameters, simultaneous formulations generally introduce Bilinear Matrix Inequality (BMI) constraints through products of plant and controller variables. In contrast with Linear Matrix Inequalities (LMIs), which can be handled efficiently using convex optimization, BMI-constrained problems are nonconvex and NP-hard, and a globally optimal solution cannot generally be guaranteed [7]. Consequently, considerable attention has been directed toward equivalent or approximate iterative LMI-based reformulations that can be solved using established interior-point algorithms [8].

LMI-based integrated design has been investigated in several aerospace applications. In [9], control-surface sizing is optimized while open- and closed-loop static and dynamic requirements are imposed as LMIs within an H_∞ framework. Necessary and sufficient solvability conditions for related formulations are derived in [10] through the introduction of auxiliary variables. The methodology is extended to multiple operating conditions in [11] by enforcing several sets of LMI constraints within an iterative procedure. In [12], aircraft and controller parameters are optimized concurrently to establish closed-loop tail-sizing criteria for a transport aircraft, including the maximum allowable aft centre-of-gravity location under flying-quality and actuator constraints. An integrated optimization of rotor and flight control system parameters for a single-main-rotor helicopter is presented in [4], with aeroelastic and handling-quality constraints based on a representative subset of ADS-33 requirements [13]. A nonlinear iterative co-design strategy is proposed in [3], demonstrating reduced conservatism relative to system-equivalence-based approaches, although its applicability is problem dependent. More recently, the authors developed an iterative LMI-based methodology for the integrated sizing and control design of a VTOL air vehicle, using an LQR formulation in [14], and using an H_∞ formulation in [15].

The present study extends this framework to a general sequential co-design methodology in which plant-design variables, controller parameters, and the parameters of a linear reference model are optimized in an integrated manner. Within an Explicit Model Following (EMF) architecture, the reference model defines the desired closed-loop dynamics and may be parameterized according to application-specific performance requirements. The framework incorporates LMI formulations of the H_2, H_∞, and mixed H_2/H_∞ state-feedback problems. Since the resulting integrated formulation gives rise to BMI constraints, a perturbation-based reformulation is introduced to decompose the problem into sequential convex LMI subproblems. This enables simultaneous updates of the plant and reference-model parameters while preserving a tractable controller synthesis procedure. The proposed methodology is demonstrated through a VTOL aircraft co-design application, in which the reference-model dynamics are selected in accordance with ADS-33 handling-quality requirements.

The proposed iterative procedure is schematically illustrated in Figure 1.

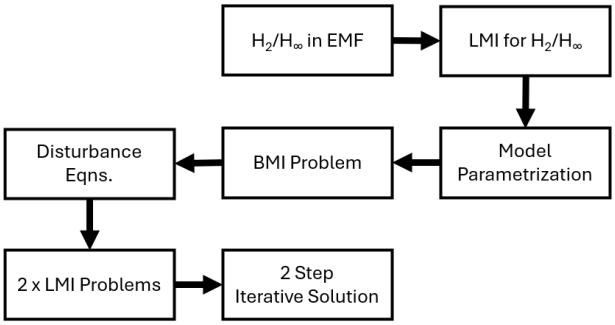


Figure 1. Overview of the proposed iterative co-design procedure.

2. Control Synthesis Framework

2.1. Model Following Control

Model Following Control (MFC) is a well-established methodology that has been successfully applied in rotorcraft flight control systems [16]. By enforcing closed-loop stability and performance through a prescribed reference model, Explicit Model Following (EMF)—a particular realization of MFC—provides a systematic and transparent framework for control-law design. Owing to these attributes, EMF is adopted in this study as an appropriate approach for the integrated control of the VTOL aircraft. In particular, an Attitude-Command Attitude-Hold (ACAH) EMF control architecture, as illustrated in Figure 2, is implemented to stabilize and control the vehicle in both hover and forward-flight conditions.

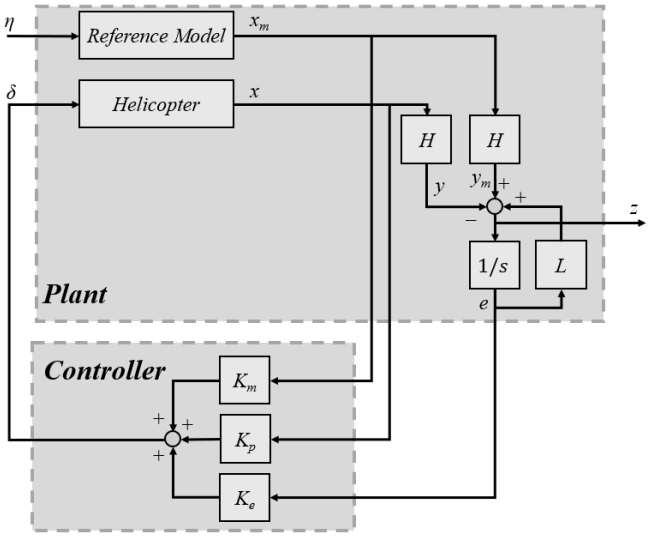


Figure 2. Explicit Model Following (EMF) control architecture.

The plant model is represented by the following linear state-space equations:

$$\begin{aligned} \dot{\mathbf{x}} &= \mathbf{A}\mathbf{x} + \mathbf{B}\delta \\ \mathbf{y} &= \mathbf{H}\mathbf{x} \end{aligned} \tag{1}$$

where $\mathbf{x}$, δ, and $\mathbf{y}$ denote the state, input and output vectors respectively.

The reference-model dynamics are described by

$$\begin{aligned} \dot{\mathbf{x}}_m &= \mathbf{A}_m\mathbf{x}_m + \mathbf{B}_m\boldsymbol{\eta} \\ \mathbf{y}_m &= \mathbf{H}\mathbf{x}_m \end{aligned} \tag{2}$$

where $\mathbf{x}_m$ denotes the reference model state vector, $\boldsymbol{\eta}$ represents the reference command input, and $\mathbf{y}_m$ is the reference-model output vector.

The tracking-error dynamics $\mathbf{e}$ are defined as

$$\dot{\mathbf{e}} = \mathbf{y}_m - \mathbf{y} + \mathbf{L}\mathbf{e} \tag{3}$$

where $\mathbf{e}$ denotes the tracking error between the reference model output and the plant output and $\mathbf{L}$ is a design matrix used to shape the error dynamics. An augmented dynamic system can be constructed using the plant model (1), the reference model (2), and the error signal dynamics (3), i.e.,

$$\begin{bmatrix} \dot{\mathbf{x}} \\ \dot{\mathbf{x}}_m \\ \dot{\mathbf{e}} \end{bmatrix} = \begin{bmatrix} \mathbf{A} & \mathbf{0} & \mathbf{0} \\ \mathbf{0} & \mathbf{A}_m & \mathbf{0} \\ -\mathbf{H} & \mathbf{H} & \mathbf{L} \end{bmatrix} \begin{bmatrix} \mathbf{x} \\ \mathbf{x}_m \\ \mathbf{e} \end{bmatrix} + \begin{bmatrix} \mathbf{0} \\ \mathbf{B}_m \\ \mathbf{0} \end{bmatrix} \boldsymbol{\eta} + \begin{bmatrix} \mathbf{B} \\ \mathbf{0} \\ \mathbf{0} \end{bmatrix} \boldsymbol{\delta} \tag{4}$$

By appropriately defining the augmented state vector $\hat{\mathbf{x}}$, the performance output z, and the system matrices $\hat{\mathbf{A}}$, $\hat{\mathbf{B}}_\eta$ and $\hat{\mathbf{B}}_\delta$, the augmented system dynamics may be expressed in the following compact form:

$$\begin{aligned} \dot{\hat{\mathbf{x}}} &= \hat{\mathbf{A}}\hat{\mathbf{x}} + \hat{\mathbf{B}}_\eta \boldsymbol{\eta} + \hat{\mathbf{B}}_\delta \boldsymbol{\delta} \\ \mathbf{z} &= \dot{\mathbf{e}} = \hat{\mathbf{C}}_z \hat{\mathbf{x}} \end{aligned} \tag{5}$$

where $\mathbf{z}$ represents the performance output.

Within this framework, a static state-feedback control law is assumed in the form

$$\boldsymbol{\delta}(t) = \mathbf{K}\hat{\mathbf{x}}(t) = \mathbf{K}_p \mathbf{x}(t) + \mathbf{K}_m \mathbf{x}_m(t) + \mathbf{K}_e \mathbf{e}(t) \tag{6}$$

where $\mathbf{K}_p$, $\mathbf{K}_m$, and $\mathbf{K}_e$ denote the gain matrices associated with the plant states, reference model states, and tracking error, respectively.

2.2. LMI Formulation of the H_2 State-Feedback Problem

Consider a generic linear system described by

$$\begin{aligned} \dot{\mathbf{x}} &= \mathbf{A}\mathbf{x} + \mathbf{B}_1 \mathbf{u} + \mathbf{B}_2 \mathbf{w} \\ \mathbf{z} &= \mathbf{C}\mathbf{x} + \mathbf{D}_1 \mathbf{u} \end{aligned} \tag{7}$$

where $\mathbf{x}$ denotes the state vector, $\mathbf{u}$ the control input, $\mathbf{w}$ an exogenous disturbance, and $\mathbf{z}$ the performance output. The objective of the H_2 control problem is to design a state-feedback control law $\mathbf{u} = \mathbf{K}\mathbf{x}$, such that the closed-loop transfer function satisfies $\|G_{\mathbf{zw}}(s)\|_2 < \gamma$ for a prescribed scalar $\gamma > 0$. This problem admits a solution if and only if there exists a matrix $\mathbf{W}$, a symmetric matrix $\mathbf{Z}$, and a symmetric positive definite matrix $\mathbf{P}$ such that the following conditions are satisfied

$$\begin{aligned} &(\mathbf{A}\mathbf{P} + \mathbf{B}_1\mathbf{W})^T + (\mathbf{A}\mathbf{P} + \mathbf{B}_1\mathbf{W}) + \mathbf{B}_2\mathbf{B}_2^T < 0 \\ &\begin{bmatrix} -\mathbf{Z} & (\mathbf{C}\mathbf{P} + \mathbf{D}_1\mathbf{W}) \\ (\mathbf{C}\mathbf{P} + \mathbf{D}_1\mathbf{W})^T & -\mathbf{P} \end{bmatrix} < 0 \\ &\mathrm{Tr}(\mathbf{Z}) - \gamma < 0 \\ &\mathbf{P} > 0 \\ &\gamma > 0 \end{aligned} \tag{8}$$

Once a feasible pair $(\mathbf{W}, \mathbf{P})$ is obtained, the corresponding state-feedback gain matrix is given by

$$\mathbf{K} = \mathbf{W}\mathbf{P}^{-1} \tag{9}$$

The optimal performance bound γ is obtained by solving the convex optimization problem

$$\begin{aligned} \min_{\mathbf{P},\mathbf{W}} \quad & \gamma \\ \text{s.t.} \quad & \text{conditions in Equation (8) are satisfied.} \end{aligned} \tag{10}$$

For the closed-loop system defined by $\mathbf{A}_c = \mathbf{A} + \mathbf{B}_1\mathbf{K}$ and $\mathbf{C}_c = \mathbf{C} + \mathbf{D}_1\mathbf{K}$, the LMI conditions can be equivalently expressed as

$$\begin{aligned} \mathbf{T}_1 &= \mathbf{P}\mathbf{A}_c^T + \mathbf{A}_c^T\mathbf{P} + \mathbf{B}_2\mathbf{B}_2^T < 0 \\ \mathbf{T}_2 &= \begin{bmatrix} -\mathbf{Z} & \mathbf{C}_c\mathbf{P} \\ \mathbf{P}\mathbf{C}_c^T & -\mathbf{P} \end{bmatrix} < 0 \\ T_3 &= \mathrm{Tr}(\mathbf{Z}) - \gamma < 0 \end{aligned} \tag{11}$$

To incorporate parametric variations, perturbations are introduced in the system and decision variables. Let $\Delta(\cdot)$ denote perturbations in the corresponding matrices, including $\Delta\mathbf{A}$, $\Delta\mathbf{B}_1$, $\Delta\mathbf{B}_2$, $\Delta\mathbf{C}$, $\Delta\mathbf{D}_1$, $\Delta\mathbf{P}$, $\Delta\mathbf{W}$, $\Delta\mathbf{Z}$, $\Delta\mathbf{T}_1$, $\Delta\mathbf{T}_2$, ΔT_3, and $\Delta\gamma$, with $\Delta\mathbf{P} = \Delta\mathbf{P}^T$ and $\Delta\mathbf{Z} = \Delta\mathbf{Z}^T$. The nominal and perturbed controller gains are constrained to be equal, such that $\mathbf{K} = \mathbf{W}\mathbf{P}^{-1} = (\mathbf{W} + \Delta\mathbf{W})(\mathbf{P} + \Delta\mathbf{P})^{-1}$.

Under these definitions, the perturbed LMI conditions can be expressed as

$$\begin{aligned} (\mathbf{T}_1 + \Delta\mathbf{T}_1) &= (\mathbf{P} + \Delta\mathbf{P})(\mathbf{A}_c + \Delta\mathbf{A}_c)^T + (\mathbf{A}_c + \Delta\mathbf{A}_c)(\mathbf{P} + \Delta\mathbf{P}) \\ &\quad + (\mathbf{B}_2 + \Delta\mathbf{B}_2)(\mathbf{B}_2 + \Delta\mathbf{B}_2)^T < 0 \\ (\mathbf{T}_2 + \Delta\mathbf{T}_2) &= \begin{bmatrix} -(\mathbf{Z} + \Delta\mathbf{Z}) & (\mathbf{C}_c + \Delta\mathbf{C}_c)(\mathbf{P} + \Delta\mathbf{P}) \\ (\mathbf{P} + \Delta\mathbf{P})(\mathbf{C}_c + \Delta\mathbf{C}_c)^T & -(\mathbf{P} + \Delta\mathbf{P}) \end{bmatrix} < 0 \\ (T_3 + \Delta T_3) &= \mathrm{Tr}(\mathbf{Z} + \Delta\mathbf{Z}) - (\gamma + \Delta\gamma) < 0 \end{aligned} \tag{12}$$

where $\Delta\mathbf{A}_c = \Delta\mathbf{A} + \Delta\mathbf{B}_1\mathbf{K}$ and $\Delta\mathbf{C}_c = \Delta\mathbf{C} + \Delta\mathbf{D}_1\mathbf{K}$.

Accordingly, the optimization problem in Equation (10) becomes

$$\begin{aligned} \min_{(\mathbf{P}+\Delta\mathbf{P},\, \mathbf{W}+\Delta\mathbf{W})} \quad & \gamma + \Delta\gamma \\ \text{s.t.} \quad & \mathbf{P} + \Delta\mathbf{P} > 0 \\ & \gamma + \Delta\gamma > 0 \\ & \mathbf{T}_1 + \Delta\mathbf{T}_1 < 0 \\ & \mathbf{T}_2 + \Delta\mathbf{T}_2 < 0 \\ & T_3 + \Delta T_3 < 0 \end{aligned} \tag{13}$$

The inequalities $\mathbf{T}_i + \Delta\mathbf{T}_i < 0, \;\; i = 1, 2, 3$ are no longer linear in variables $\mathbf{P}$, $\Delta\mathbf{P}$, $\mathbf{Z}$, $\Delta\mathbf{Z}$, $\mathbf{W}$ and $\Delta\mathbf{W}$. The perturbation terms $\Delta\mathbf{T}_i$ can be explicitly extracted from Equation (12) as

$$\begin{aligned} \Delta\mathbf{T}_1 &= \mathbf{A}_c\Delta\mathbf{P} + \Delta\mathbf{A}_c\mathbf{P} + \mathbf{P}\Delta\mathbf{A}_c^T + \Delta\mathbf{P}\mathbf{A}_c^T + \mathbf{B}_2\Delta\mathbf{B}_2^T + \Delta\mathbf{B}_2\mathbf{B}_2^T \\ &\quad + \Delta\mathbf{B}_2\Delta\mathbf{B}_2^T + \Delta\mathbf{A}_c\Delta\mathbf{P} + \Delta\mathbf{P}\Delta\mathbf{A}_c^T < 0 \\ \Delta\mathbf{T}_2 &= \begin{bmatrix} -\Delta\mathbf{Z} & \mathbf{C}_c\Delta\mathbf{P} + \Delta\mathbf{C}_c\mathbf{P} + \Delta\mathbf{C}_c\Delta\mathbf{P} \\ (\mathbf{C}_c\Delta\mathbf{P} + \Delta\mathbf{C}_c\mathbf{P} + \Delta\mathbf{C}_c\Delta\mathbf{P})^T & -\Delta\mathbf{P} \end{bmatrix} < 0 \\ \Delta T_3 &= \mathrm{Tr}(\Delta\mathbf{Z}) - (\Delta\gamma) < 0 \end{aligned} \tag{14}$$

The resulting optimization problem contains BMI constraints because of the presence of second-order perturbation terms. Two convexification strategies are considered to address this nonconvexity.

(1) Assuming all perturbations are sufficiently small, second-order terms can be neglected, yielding the first-order approximations

$$\begin{aligned}\Delta\mathbf{T}_1 \backsimeq \Delta\tilde{\mathbf{T}}_1 &= \mathbf{A}_c\Delta\mathbf{P} + \Delta\mathbf{A}_c\mathbf{P} + \mathbf{P}\Delta\mathbf{A}_c^T + \Delta\mathbf{P}\mathbf{A}_c^T + \mathbf{B}_2\Delta\mathbf{B}_2^T + \Delta\mathbf{B}_2\mathbf{B}_2^T \\ \Delta\mathbf{T}_2 \backsimeq \Delta\tilde{\mathbf{T}}_2 &= \begin{bmatrix} -\Delta\mathbf{Z} & \mathbf{C}_c\Delta\mathbf{P} + \Delta\mathbf{C}_c\mathbf{P} \\ (\mathbf{C}_c\Delta\mathbf{P} + \Delta\mathbf{C}_c\mathbf{P})^T & -\Delta\mathbf{P} \end{bmatrix}\end{aligned} \tag{15}$$

To restrict the magnitude of the perturbations, a constraint is imposed on the perturbation matrices of the form

$$\bar{\sigma}(\Delta\cdot) < \epsilon\bar{\sigma}(\cdot) \tag{16}$$

where $\bar{\sigma}(\cdot)$ denotes the maximum singular value of a given matrix (e.g., ΔP), and ϵ is a user-selected scalar satisfying $0 < \epsilon < 1$. This bound can be equivalently expressed as the following linear matrix inequality [7].

$$\begin{bmatrix} \epsilon\bar{\sigma}(\cdot)I & \Delta\cdot \\ (\Delta\cdot)^T & \epsilon\bar{\sigma}(\cdot)I \end{bmatrix} > 0 \tag{17}$$

Since restricting the perturbation magnitude does not, by itself, guarantee feasibility when second-order terms are neglected, the original BMI constraints are evaluated after each update and incorporated into the stopping criterion. If these constraints are violated, a backtracking procedure is applied using the second-order terms evaluated at the previous iteration.

(2) Alternatively, quadratic inequalities and the Schur complement are used to construct upper bounds for the perturbation terms. This procedure yields a conservative convex LMI representation that preserves the feasibility of the perturbed constraints.

Starting from the inequality

$$\begin{aligned}(\Delta\mathbf{P} - \Delta\mathbf{A}_c)(\Delta\mathbf{P} - \Delta\mathbf{A}_c)^T &\geq 0 \\ \Delta\mathbf{P}\Delta\mathbf{P} - \Delta\mathbf{P}(\Delta\mathbf{A}_c)^T - \Delta\mathbf{A}_c\Delta\mathbf{P} + \Delta\mathbf{A}_c(\Delta\mathbf{A}_c)^T &\geq 0 \\ \Delta\mathbf{P}\Delta\mathbf{P} + \Delta\mathbf{A}_c(\Delta\mathbf{A}_c)^T &\geq \Delta\mathbf{P}(\Delta\mathbf{A}_c)^T + \Delta\mathbf{A}_c\Delta\mathbf{P}\end{aligned} \tag{18}$$

an upper bound on the cross terms can be established. Defining

$$\begin{aligned}\Delta\bar{\mathbf{T}}_1 = \mathbf{A}_c\Delta\mathbf{P} + \Delta\mathbf{A}_c\mathbf{P} + \mathbf{P}(\Delta\mathbf{A}_c)^T + \Delta\mathbf{P}\mathbf{A}_c^T + \mathbf{B}_2(\Delta\mathbf{B}_2)^T + \Delta\mathbf{B}_2\mathbf{B}_2^T \\ + \Delta\mathbf{B}_2\Delta\mathbf{B}_2^T + \Delta\mathbf{A}_c(\Delta\mathbf{A}_c)^T + \Delta\mathbf{P}\Delta\mathbf{P}\end{aligned} \tag{19}$$

it follows that $\Delta\mathbf{T}_1 \leq \Delta\bar{\mathbf{T}}_1$. Enforcing $\Delta\bar{\mathbf{T}}_1 \leq 0$ therefore guarantees $\Delta\mathbf{T}_1 \leq 0$. Using the Schur complement, Equation (19) can be rewritten as

$$\Delta\bar{\mathbf{T}}_1 = \begin{bmatrix} \boldsymbol{\Xi} & * & * & * \\ -(\Delta\mathbf{B}_2)^T & -\mathbf{I} & * & * \\ -(\Delta\mathbf{A}_c)^T & 0 & -\mathbf{I} & * \\ -\Delta\mathbf{P} & 0 & 0 & -\mathbf{I} \end{bmatrix} \tag{20}$$

where

$$\boldsymbol{\Xi} = \mathbf{A}_c\Delta\mathbf{P} + \Delta\mathbf{A}_c\mathbf{P} + \mathbf{P}(\Delta\mathbf{A}_c)^T + \Delta\mathbf{P}\mathbf{A}_c^T + \mathbf{B}_2(\Delta\mathbf{B}_2)^T + \Delta\mathbf{B}_2\mathbf{B}_2^T$$

If the perturbations are affine functions of a parameter vector σ, i.e., $\Delta\mathbf{A} = \sum_{i=1}^{n} \Delta\mathbf{A}_i \sigma_i$, the BMI-constrained problem can be decomposed into two sequential LMI optimization problems. The first corresponds to the nominal H_2 synthesis (10), while the second involves the optimization of perturbations and design parameters:

$$\begin{aligned} \min_{(\Delta\mathbf{P},\,\sigma)} \quad & J(\boldsymbol{\sigma}) \\ \text{s.t.} \quad & \mathbf{P} + \Delta\mathbf{P} > 0 \\ & \gamma + \Delta\gamma > 0 \\ & \Delta\mathbf{T}_1,\ \Delta\mathbf{T}_2,\ \Delta T_3 \leq 0 \end{aligned} \tag{21}$$

2.3. LMI Formulation of the H_∞ State-Feedback Problem

For the linear system defined in Equation (7), the H_∞ control problem aims to design a state-feedback control law $\mathbf{u} = \mathbf{K}\mathbf{x}$ such that the closed-loop transfer function satisfies $\|G_{\mathbf{zw}}(s)\|_\infty < \gamma$ for a prescribed scalar $\gamma > 0$. This problem admits a solution if and only if there exist a matrix $\mathbf{W}$ and a symmetric positive definite matrix $\mathbf{P}$ such that the following LMIs hold:

$$\begin{aligned} \mathbf{T} = \begin{bmatrix} (\mathbf{A}\mathbf{P} + \mathbf{B}_1\mathbf{W})^T + (\mathbf{A}\mathbf{P} + \mathbf{B}_1\mathbf{W}) & \mathbf{B}_2 & (\mathbf{C}\mathbf{P} + \mathbf{D}_1\mathbf{W})^T \\ \mathbf{B}_2^T & -\gamma\mathbf{I} & 0 \\ \mathbf{C}\mathbf{P} + \mathbf{D}_1\mathbf{W} & 0 & -\gamma\mathbf{I} \end{bmatrix} < 0 \\ \mathbf{P} > 0 \\ \gamma > 0 \end{aligned} \tag{22}$$

and the state-feedback gain matrix is computed as $\mathbf{K} = \mathbf{W}\mathbf{P}^{-1}$. The minimum achievable value of γ can be determined by solving the following convex optimization problem:

$$\begin{aligned} \min_{\mathbf{P},\,\mathbf{W}} \quad & \gamma \\ \text{s.t.} \quad & \text{conditions in Equation (22) are satisfied.} \end{aligned} \tag{23}$$

For the state-feedback control law $\mathbf{u} = \mathbf{K}\mathbf{x}$, the closed-loop system matrices $\mathbf{A}_c$ and $\mathbf{C}_c$ are defined as in the previous case, and the LMI condition in Equation (22) can be equivalently rewritten as

$$\mathbf{T} = \begin{bmatrix} \mathbf{P}\mathbf{A}_c^T + \mathbf{A}_c\mathbf{P} & \mathbf{B}_2 & \mathbf{P}\mathbf{C}_c^T \\ \mathbf{B}_2^T & -\gamma\mathbf{I} & 0 \\ \mathbf{C}_c\mathbf{P} & 0 & -\gamma\mathbf{I} \end{bmatrix} \tag{24}$$

Defining the perturbations in matrix $\Delta\mathbf{T}$ and its parameters, and following a similar procedure as in the previous section, we can come up with a perturbation equation:

(1) As in the H_2 formulation, the perturbations are assumed to be sufficiently small such that second-order terms can be neglected. This yields the first-order approximation

$$\Delta\mathbf{T} \backsimeq \Delta\tilde{\mathbf{T}} = \begin{bmatrix} \mathbf{A}_c\Delta\mathbf{P} + \Delta\mathbf{P}\mathbf{A}_c^T + \mathbf{P}(\Delta\mathbf{A}_c)^T + \Delta\mathbf{A}_c\mathbf{P} & * & * \\ (\Delta\mathbf{B}_2)^T & -\Delta\gamma\mathbf{I} & * \\ \mathbf{C}_c\Delta\mathbf{P} + \Delta\mathbf{C}_c\mathbf{P} & \Delta\mathbf{D}_2 & -\Delta\gamma\mathbf{I} \end{bmatrix} \tag{25}$$

To limit the magnitude of the perturbations, the perturbation-magnitude constraint given in Equation (17) is imposed [7]. In addition, the original BMI constraints are evaluated after each update and included in the stopping criterion. When necessary, a backtracking procedure analogous to that employed in the H_2 formulation is applied.

(2) Alternatively, defining $\Delta\bar{\mathbf{T}}$ based on Equation (18) and applying the Schur complement yields

$$\Delta\bar{\mathbf{T}} = \begin{bmatrix} \mathbf{A}_c\Delta\mathbf{P} + \Delta\mathbf{P}\mathbf{A}_c^T + \mathbf{P}(\Delta\mathbf{A}_c)^T + \Delta\mathbf{A}_c\mathbf{P} & * & * & * & * \\ -(\Delta\mathbf{A}_c)^T & -\mathbf{I} & * & * & * \\ -\Delta\mathbf{P} & 0 & -\mathbf{I} & * & * \\ (\Delta\mathbf{B}_2)^T & 0 & 0 & -\Delta\gamma\mathbf{I} & * \\ \mathbf{C}_c\Delta\mathbf{P} + \Delta\mathbf{C}_c\mathbf{P} + \Delta\mathbf{C}_c\Delta\mathbf{P} & 0 & 0 & 0 & -\Delta\gamma\mathbf{I} \end{bmatrix} \tag{26}$$

it follows that $\Delta\mathbf{T} \leq \Delta\bar{\mathbf{T}}$. Therefore, enforcing, $\Delta\bar{\mathbf{T}} \leq 0$ provides a sufficient condition for $\Delta\mathbf{T} \leq 0$. In the particular case where $\Delta\mathbf{C}_c = 0$, the matrix $\Delta\bar{\mathbf{T}}$ is convex and can therefore be employed in the subsequent derivations.

If the perturbations depend affinely on a parameter vector $\sigma = [\sigma_1, \ldots, \sigma_n]^T$, the resulting BMI-constrained problem can be decomposed into two sequential LMI optimization problems. The first corresponds to the nominal H_∞ synthesis, while the second addresses the perturbation variables:

$$\begin{aligned} \min_{(\Delta\mathbf{P},\,\sigma)} \quad & J(\sigma) \\ \text{s.t.} \quad & \mathbf{P} + \Delta\mathbf{P} > 0 \\ & \gamma + \Delta\gamma > 0 \\ & \Delta\mathbf{T} \leq 0 \end{aligned} \tag{27}$$

2.4. Extension to Multiple Design Points

For two distinct design points, denoted by the subscripts $(\cdot)_a$ and $(\cdot)_b$, consider the generalized linear systems

$$\begin{aligned} \dot{\mathbf{x}} &= \mathbf{A}_a\mathbf{x} + \mathbf{B}_{a1}\mathbf{u} + \mathbf{B}_{a2}\mathbf{w} \\ \mathbf{z} &= \mathbf{C}_a\mathbf{x} + \mathbf{D}_{a1}\mathbf{u} \end{aligned} \tag{28}$$

and

$$\begin{aligned} \dot{\mathbf{x}} &= \mathbf{A}_b\mathbf{x} + \mathbf{B}_{b1}\mathbf{u} + \mathbf{B}_{b2}\mathbf{w} \\ \mathbf{z} &= \mathbf{C}_b\mathbf{x} + \mathbf{D}_{b1}\mathbf{u} \end{aligned} \tag{29}$$

The multi-design-point H_∞ state-feedback problem seeks a single gain matrix $\mathbf{K}$ such that the closed-loop transfer functions from $\mathbf{w}$ to $\mathbf{z}$ satisfy $\|G_{\mathbf{zw}}(s)\|_\infty < \gamma$ at both operating points. A solution exists if and only if there exist a symmetric positive definite matrix $\mathbf{P}$ and a matrix $\mathbf{W}$, such that Equation (24) holds for both $\mathbf{T}_a$ and $\mathbf{T}_b$. Given any feasible pair ($\mathbf{W}$,$\mathbf{P}$), the corresponding state-feedback gain is recovered as $\mathbf{K} = \mathbf{W}\mathbf{P}^{-1}$. The minimum achievable performance level γ is then obtained by solving the convex optimization problem in (23), subject to $\mathbf{T}_a < 0$ and $\mathbf{T}_b < 0$.

Following the same development as in the previous subsection, the formulation can equivalently be expressed in terms of the disturbance terms $\Delta\mathbf{T}_a$ and $\Delta\mathbf{T}_b$. In this case, the optimization problem (27) is solved under the constraints $\Delta\mathbf{T}_a < 0$ and $\Delta\mathbf{T}_b < 0$.

Although straightforward to implement, the multiple-point design formulation introduces additional conservatism by requiring a common set of plant and controller variables to satisfy the prescribed stability and performance constraints simultaneously across all selected operating conditions. Further conservatism may arise from the use of common Lyapunov or auxiliary variables across the design points. As a result, the feasible region is restricted to the intersection of the individual design-point feasible sets, which may limit the achievable improvement, particularly when the preferred design directions differ across operating conditions.

2.5. LMI Formulation of the Mixed H_∞/H_2 State-Feedback Problem

Consider a generic linear time-invariant system described by the state-space equations

$$\begin{aligned} \dot{\mathbf{x}} &= \mathbf{A}\mathbf{x} + \mathbf{B}_1\mathbf{u} + \mathbf{B}_2\mathbf{w} \\ \mathbf{z}_\infty &= \mathbf{C}_\infty\mathbf{x} + \mathbf{D}_{\infty 1}\mathbf{u} \\ \mathbf{z}_2 &= \mathbf{C}_2\mathbf{x} + \mathbf{D}_{21}\mathbf{u} \end{aligned} \tag{30}$$

where $\mathbf{x}$, $\mathbf{u}$, and $\mathbf{w}$ denote the state vector, control input, and exogenous disturbance, respectively. The outputs $\mathbf{z}_\infty$ and $\mathbf{z}_2$ correspond to the H_∞ and H_2 performance channels.

For a state-feedback control law $\mathbf{u} = \mathbf{K}\mathbf{x}$, the mixed H_∞/H_2 synthesis problem is to determine a gain matrix $\mathbf{K}$, such that the closed-loop system satisfies

$$\|G_{\mathbf{z}_\infty \mathbf{w}}(s)\|_\infty < \gamma_\infty \qquad \|G_{\mathbf{z}_2 \mathbf{w}}(s)\|_2 < \gamma_2$$

for positive scalars γ_∞ and γ_2. This problem is feasible if and only if there exist a matrix $\mathbf{W}$, a symmetric positive definite matrix $\mathbf{P}$, and a symmetric matrix $\mathbf{Z}$, such that the LMIs in (8) and (22) are satisfied simultaneously. Given any feasible triple $(\mathbf{P}, \mathbf{W}, \mathbf{Z})$, the corresponding state-feedback gain is recovered as $\mathbf{K} = \mathbf{W}\mathbf{P}^{-1}$. A common design objective is to minimize a weighted combination of the H_2 and H_∞ performance levels, which leads to the convex optimization problem

$$\begin{aligned} \min_{(\mathbf{P},\mathbf{W},\mathbf{Z})} \quad & c_2\gamma_2 + c_\infty\gamma_\infty \\ & \text{s.t. the inequalities of Equations (8) and (22) hold} \\ & c_2 > 0, \;\; c_\infty > 0 \end{aligned} \tag{31}$$

Imposing the structural assumptions $\mathbf{C} = \mathbf{C}_\infty = \mathbf{C}_2$, $\mathbf{D}_1 = \mathbf{D}_{\infty 1} = \mathbf{D}_{21}$, and $\mathbf{D}_{\infty 2} = 0$, a unified regulated output $\mathbf{z}_\infty = \mathbf{z}_2 = \mathbf{z}$ is obtained. Under this assumption, and following the perturbation-based development used for the individual H_∞ and H_2 formulations, variations are introduced on the plant matrices and decision variables. The resulting mixed H_2/H_∞ formulation then follows the same structure as the cases presented in the preceding sections.

A comprehensive assessment on the LMI formulations for the H_2, H_∞ and mixed H_2/H_∞ synthesis problems is provided in Ref. [17].

The proposed mixed H_2/H_∞ formulation introduces additional conservatism due to the supplementary constraints and the use of convex LMI conditions, which provide sufficient conditions for simultaneously satisfying the two performance objectives. As a result, the feasible set of the convex formulation is generally more restrictive than that of the original BMI-constrained problem. This conservatism may reduce the achievable improvement in both the plant and controller design variables, particularly when the H_2 and H_∞ objectives are conflicting.

2.6. Model Parametrization

Let $\boldsymbol{\sigma}$ denote the vector of normalized aircraft design variables to be optimized, with each component constrained within the interval $-1 \le \sigma_i \le 1$. To capture the dependence of the linearized system dynamics on the underlying physical design parameters, the state-space matrices are expressed as affine functions of $\boldsymbol{\sigma}$. Specifically,

$$\mathbf{A}(\boldsymbol{\sigma}) = \mathbf{A}_0 + \sum_{i=1}^{n} \mathbf{A}_i\sigma_i \qquad \mathbf{B}(\boldsymbol{\sigma}) = \mathbf{B}_0 + \sum_{i=1}^{n} \mathbf{B}_i\sigma_i \tag{32}$$

where $\mathbf{A}_0$ and $\mathbf{B}_0$ denote the nominal system matrices, and $\mathbf{A}_i$ and $\mathbf{B}_i$ represent the sensitivity matrices associated with the ith design variable. This affine parametrization provides a compact representation of plant variability over the normalized design space and is well suited for LMI-based controller synthesis and integrated optimization.

Similarly, the reference-model matrices $(\mathbf{A}_m, \mathbf{B}_m)$ can be parameterized in terms of a set of normalized reference-model parameters ν_j, subject to the bounds $-1 \leq \nu_j \leq 1$. In the present application, these parameters are defined as functions of the natural frequencies associated with the corresponding motion axes, i.e., $\nu_j = f(\omega_{nj})$, where j denotes the motion axis (e.g., pitch, roll, yaw, or heave). This formulation enables systematic variation of the reference model dynamics through physically meaningful modal characteristics while preserving compatibility with the normalized optimization framework:

$$\mathbf{A}_m(\boldsymbol{\nu}) = \mathbf{A}_{m0} + \sum_{j=1}^{k} \mathbf{A}_{mj}\nu_j \qquad \mathbf{B}_m(\boldsymbol{\nu}) = \mathbf{B}_{m0} + \sum_{j=1}^{k} \mathbf{B}_{mj}\nu_j \tag{33}$$

The augmented parametric model in Equation (4) may therefore be written in the compact state-space form

$$\begin{aligned} \dot{\hat{\mathbf{x}}} &= \hat{\mathbf{A}}(\boldsymbol{\sigma}, \boldsymbol{\nu})\hat{\mathbf{x}} + \hat{\mathbf{B}}_\eta(\boldsymbol{\nu})\boldsymbol{\eta} + \hat{\mathbf{B}}_\delta(\boldsymbol{\sigma})\boldsymbol{\delta} \\ \mathbf{z} &= \hat{\mathbf{C}}_z\hat{\mathbf{x}} \end{aligned}$$

where the augmented system matrices depend affinely on the design variables $\boldsymbol{\sigma}$ and the reference-model parameters $\boldsymbol{\nu}$:

$$\begin{aligned} \hat{\mathbf{A}}(\boldsymbol{\sigma}, \boldsymbol{\nu}) &= \hat{\mathbf{A}}_0 + \sum_{i=1}^{n} \hat{\mathbf{A}}_i\sigma_i + \sum_{j=1}^{k} \hat{\mathbf{A}}_{mj}\nu_j \\ \hat{\mathbf{B}}_\eta(\boldsymbol{\nu}) &= \hat{\mathbf{B}}_{\eta 0} + \sum_{j=1}^{k} \hat{\mathbf{B}}_{\eta j}\nu_j \\ \hat{\mathbf{B}}_\delta(\boldsymbol{\sigma}) &= \hat{\mathbf{B}}_{\delta 0} + \sum_{i=1}^{n} \hat{\mathbf{B}}_{\delta i}\sigma_i \end{aligned} \tag{34}$$

The corresponding nominal and sensitivity matrices are defined as

$$\begin{aligned} \hat{\mathbf{A}}_0 &= \begin{bmatrix} \mathbf{A}_0 & 0 & 0 \\ 0 & \mathbf{A}_{m0} & 0 \\ -\mathbf{H} & \mathbf{H} & \mathbf{L} \end{bmatrix} \quad \hat{\mathbf{A}}_i = \begin{bmatrix} \mathbf{A}_i & 0 & 0 \\ 0 & 0 & 0 \\ 0 & 0 & 0 \end{bmatrix} \quad \hat{\mathbf{A}}_{mj} = \begin{bmatrix} 0 & 0 & 0 \\ 0 & \mathbf{A}_{mj} & 0 \\ 0 & 0 & 0 \end{bmatrix} \\ \hat{\mathbf{B}}_{\eta 0} &= \begin{bmatrix} 0 \\ \mathbf{B}_{m0} \\ 0 \end{bmatrix} \quad \hat{\mathbf{B}}_{\eta j} = \begin{bmatrix} 0 \\ \mathbf{B}_{mj} \\ 0 \end{bmatrix} \quad \hat{\mathbf{B}}_{\delta 0} = \begin{bmatrix} \mathbf{B}_0 \\ 0 \\ 0 \end{bmatrix} \quad \hat{\mathbf{B}}_{\delta i} = \begin{bmatrix} \mathbf{B}_i \\ 0 \\ 0 \end{bmatrix} \quad \hat{\mathbf{C}}_z = \begin{bmatrix} -\mathbf{H} \\ \mathbf{H} \\ \mathbf{L} \end{bmatrix}^T \end{aligned} \tag{35}$$

3. Iterative Co-Design Procedure

An iterative procedure is employed for the sequential optimization of the control system and design variables. The algorithm follows the framework introduced in Section 2 and alternates between controller synthesis and plant-parameter updates. The composite objective function is defined as a weighted sum of the controller synthesis cost γ and the cost associated with the vehicle design parameters $\boldsymbol{\sigma}$. In order to balance the objectives, a normalized row-inverse Jacobian, $\mathbf{J}_{inv}$, can be used in conjunction with a user-defined weighting vector $\mathbf{W}$, yielding

$$C = (\gamma + \mathbf{W}\mathbf{J}_{inv}\boldsymbol{\sigma})$$

The steps of the proposed algorithm are summarized below.

Integrated Plant–Controller Optimization Procedure

1. Initialization.
   Initialize the design variables and reference-model parameters as $\boldsymbol{\sigma} = 0$ and $\boldsymbol{\nu} = 0$. Compute the matrices $\hat{\mathbf{A}}_0$, $\hat{\mathbf{B}}_{u0}$, $\hat{\mathbf{B}}_{w0}$, $\hat{\mathbf{A}}_i$, $\hat{\mathbf{B}}_{ui}$, $\hat{\mathbf{A}}_{mj}$, and $\hat{\mathbf{B}}_{wmj}$ from (35). Initialize the auxiliary matrices as
   $$\hat{\mathbf{A}}_s = \hat{\mathbf{A}}_0; \;\; \hat{\mathbf{B}}_s = \hat{\mathbf{B}}_0$$
2. Controller synthesis for fixed parameters.
   For fixed values of $(\boldsymbol{\sigma}, \boldsymbol{\nu})$, solve the LMI optimization problem to determine $\mathbf{P}$ and $\mathbf{W}$ by minimizing γ subject to the constraint set.
3. Closed-loop realization.
   Compute the state-feedback gain and the closed-loop system matrices as
   $$\begin{aligned} \mathbf{K} &= \mathbf{W}\mathbf{P}^{-1} \\ \hat{\mathbf{A}}_c &= \hat{\mathbf{A}}_s + \hat{\mathbf{B}}_s\mathbf{K} \\ \hat{\mathbf{A}}_{ic} &= \hat{\mathbf{A}}_i + \hat{\mathbf{B}}_i\mathbf{K} \end{aligned}$$
4. Plant-parameter update (fixed $\mathbf{K}$).
   For fixed controller gain $\mathbf{K}$, solve the LMI optimization problem to determine $\Delta\boldsymbol{\sigma}$, $\Delta\boldsymbol{\nu}$, $\Delta\mathbf{P}$, and $\Delta\gamma$ subject to the prescribed LMI constraints, including the positive definiteness condition $\mathbf{P} + \Delta\mathbf{P} > 0$, the bounds on $\boldsymbol{\sigma}$ and $\boldsymbol{\nu}$, and the closed-loop performance constraints.
5. Parameter update.
   Update the design variables and reference-model parameters as
   $$\boldsymbol{\sigma} + \Delta\boldsymbol{\sigma} \to \boldsymbol{\sigma} \qquad \boldsymbol{\nu} + \Delta\boldsymbol{\nu} \to \boldsymbol{\nu}$$
   Recompute the auxiliary matrices $\hat{\mathbf{A}}_s$, $\hat{\mathbf{B}}_s$, and $\hat{\mathbf{B}}_{\eta 0}$ accordingly.
   $$\begin{aligned} \hat{\mathbf{A}}_s + \sum_{i=1}^{n} \hat{\mathbf{A}}_i \Delta\sigma_i + \sum_{j=1}^{k} \hat{\mathbf{A}}_{mj} \Delta\nu_j &\to \hat{\mathbf{A}}_s \\ \hat{\mathbf{B}}_s + \sum_{i=1}^{n} \hat{\mathbf{B}}_i \Delta\sigma_i &\to \hat{\mathbf{B}}_s \\ \hat{\mathbf{B}}_{\eta 0} + \sum_{j=1}^{k} \hat{\mathbf{B}}_{mj} \Delta\nu_j &\to \hat{\mathbf{B}}_{\eta 0} \end{aligned}$$
6. Convergence check.
   If the convergence criteria on γ, $\boldsymbol{\sigma}$, and $\boldsymbol{\nu}$ are satisfied, terminate the algorithm; otherwise, return to Step 2.

4. VTOL Air Vehicle Example

In this section, the proposed co-design methodology is applied to the sizing of a VTOL air vehicle. A quad-wing tilt-rotor VTOL aircraft, comprising a fuselage, wing, horizontal tail, and four identical rotors, is considered as the baseline configuration. The rotors are mounted at the tips of the wing and horizontal tail and are assumed to operate at a constant rotational speed. The rotor arrangement is symmetric about the body x-axis, and, under hover conditions, the resultant rotor lift is assumed to act through the aircraft center of gravity.

Vehicle control is achieved through differential variation of the individual rotor blade-pitch angles. No conventional aerodynamic control surfaces, such as elevators, ailerons, or rudders, are incorporated. Furthermore, the configuration does not include a vertical tail; hence, directional control is provided exclusively by the rotors. For modeling purposes, the wing and horizontal tail are represented by rectangular planforms with symmetric airfoil sections. The baseline vehicle configuration is illustrated in Figure 3.



Figure 3. Tilt-rotor VTOL quad-wing air vehicle.

4.1. Air Vehicle (Plant) Model

Linear parametric models that capture the aircraft dynamics are required to support the integrated plant–controller design process. To derive these linear representations, a set of representative nonlinear dynamic models is first constructed by assembling the individual vehicle components, including the wing, horizontal tail, fuselage, and rotors. For this purpose, a publicly available generic single-main-rotor helicopter mathematical model [18,19] is extended to represent the multirotor configuration considered in this study. The rotor model structure is replicated for each rotor, while analogous formulations are introduced for the fuselage, wing, and horizontal tail. A schematic representation of the nonlinear model is presented in Figure 4.

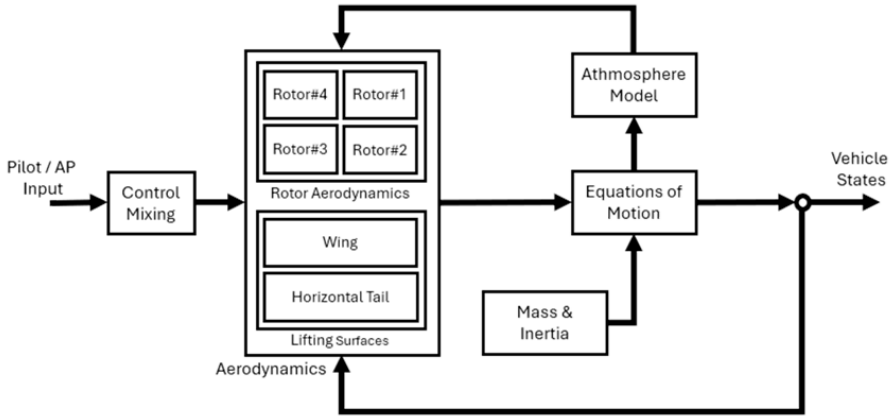


Figure 4. Non-linear air vehicle model components.

The complete nonlinear model is implemented in MATLAB/Simulink R2024a, with key geometric and aerodynamic parameters—such as wing and tail dimensions, rotor radius, rotor placement, and rotor incidence angles—defined explicitly as parametric variables. Dedicated scripts are developed to trim the nonlinear model, perform linearization about the trimmed operating conditions, and extract linear parametric state-space representations corresponding to the selected set of design variables.

Once the trim condition has been obtained, the linearized model about the corresponding operating point is constructed by evaluating the Jacobian matrix at the trim equilibrium. The resulting linearized vehicle dynamics can be expressed in state-space form as $\dot{\mathbf{x}} = \mathbf{A}\mathbf{x} + \mathbf{B}\boldsymbol{\delta}$, where the state and control input vectors are defined as

$$\begin{aligned} \mathbf{x} &= \begin{bmatrix} u & w & q & \theta & v & p & \phi & r \end{bmatrix}^T \\ \boldsymbol{\delta} &= \begin{bmatrix} \delta_{col} & \delta_{lon} & \delta_{lat} & \delta_{ped} \end{bmatrix}^T \end{aligned} \tag{36}$$

The system matrices **A** and **B** are composed of dimensional stability and control derivatives evaluated at the trim condition. The state matrix **A** is given by

$$\mathbf{A} = \begin{bmatrix} X_u & X_w & X_q & -gc(\theta_e) & X_v & X_p & 0 & X_r \\ Z_u & Z_w & Z_q & -gc(\phi_e)s(\theta_e) & Z_v & Z_p & -gs(\phi_e)c(\theta_e) & Z_r \\ M_u & M_w & M_q & 0 & M_v & M_p & 0 & M_r \\ 0 & 0 & 1 & 0 & 0 & 0 & 0 & -s(\phi_e) \\ Y_u & Y_w & Y_q & -gs(\phi_e)s(\theta_e) & Y_v & Y_p & gc(\phi_e)c(\theta_e) & Y_r \\ L_u & L_w & L_q & 0 & L_v & L_p & 0 & L_r \\ 0 & 0 & s(\phi_e)t(\theta_e) & 0 & 0 & 1 & 0 & c(\phi_e)t(\theta_e) \\ N_u & N_w & N_q & 0 & N_v & N_p & 0 & N_r \end{bmatrix} \tag{37}$$

and the input matrix **B** is defined as

$$\mathbf{B} = \begin{bmatrix} X_{\delta_{col}} & X_{\delta_{lon}} & X_{\delta_{lat}} & X_{\delta_{ped}} \\ Z_{\delta_{col}} & Z_{\delta_{lon}} & Z_{\delta_{lat}} & Z_{\delta_{ped}} \\ M_{\delta_{col}} & M_{\delta_{lon}} & M_{\delta_{lat}} & M_{\delta_{ped}} \\ 0 & 0 & 0 & 0 \\ Y_{\delta_{col}} & Y_{\delta_{lon}} & Y_{\delta_{lat}} & Y_{\delta_{ped}} \\ L_{\delta_{col}} & L_{\delta_{lon}} & L_{\delta_{lat}} & L_{\delta_{ped}} \\ 0 & 0 & 0 & 0 \\ N_{\delta_{col}} & N_{\delta_{lon}} & N_{\delta_{lat}} & N_{\delta_{ped}} \end{bmatrix} \tag{38}$$

Here $c(\cdot)$, $s(\cdot)$, and $t(\cdot)$ denote the shorthand notations for $\cos(\cdot)$, $\sin(\cdot)$, and $\tan(\cdot)$, respectively.

The system and input matrices can be partitioned as

$$\mathbf{A} = \begin{bmatrix} \mathbf{A}_{\text{lon}} & \mathbf{A}_{\text{c1}} \\ \mathbf{A}_{\text{c2}} & \mathbf{A}_{\text{lat}} \end{bmatrix}, \qquad \mathbf{B} = \begin{bmatrix} \mathbf{B}_{\text{lon}} & \mathbf{B}_{\text{c1}} \\ \mathbf{B}_{\text{c2}} & \mathbf{B}_{\text{lat}} \end{bmatrix}, \tag{39}$$

where $\mathbf{A}_{\text{c1}}$, $\mathbf{A}_{\text{c2}}$, $\mathbf{B}_{\text{c1}}$, and $\mathbf{B}_{\text{c2}}$ represent the coupling terms between longitudinal and lateral-directional dynamics.

The coupling between longitudinal and lateral-directional dynamic modes is considered weak when the differences in modal characteristics—namely, natural frequency and damping ratio—between the full-order and reduced-order models remain sufficiently small. Unlike conventional helicopters, the quad-wing configuration exhibits relatively reduced inter-axis coupling between the longitudinal and lateral-directional dynamics. For small trim angles, $\theta_e \approx 0$ and $\phi_e \approx 0$, and under the assumption that the coupling terms are negligible, the system can be approximated by decoupled longitudinal and lateral-directional subsystems.

$$\mathbf{A}_{\text{lon}} = \begin{bmatrix} X_u & X_w & X_q & -g \\ Z_u & Z_w & Z_q & 0 \\ M_u & M_w & M_q & 0 \\ 0 & 0 & 1 & 0 \end{bmatrix} \quad \mathbf{B}_{\text{lon}} = \begin{bmatrix} X_{\delta_{\text{col}}} & X_{\delta_{\text{lon}}} \\ Z_{\delta_{\text{col}}} & Z_{\delta_{\text{lon}}} \\ M_{\delta_{\text{col}}} & M_{\delta_{\text{lon}}} \\ 0 & 0 \end{bmatrix}$$
$$\mathbf{A}_{\text{lat}} = \begin{bmatrix} Y_v & Y_p & g & Y_r \\ L_v & L_p & 0 & L_r \\ 0 & 1 & 0 & 0 \\ N_v & N_p & 0 & N_r \end{bmatrix} \quad \mathbf{B}_{\text{lat}} = \begin{bmatrix} Y_{\delta_{\text{lat}}} & Y_{\delta_{\text{ped}}} \\ L_{\delta_{\text{lat}}} & L_{\delta_{\text{ped}}} \\ 0 & 0 \\ N_{\delta_{\text{lat}}} & N_{\delta_{\text{ped}}} \end{bmatrix} \tag{40}$$

As noted previously, vehicle control is realized through individual actuation of the rotor blade pitch angles. The commanded blade pitch for each rotor is obtained through control mixing of the pilot or controller inputs associated with the heave, roll, pitch, and yaw axes. This control mixing is implemented using a multirotor coordinate transformation applied to the control input vector defined in Equation (41). In this formulation, δ_{col} denotes the collective input governing vertical (heave) motion, δ_{lat} and δ_{lon} represent the lateral and longitudinal cyclic inputs associated with roll and pitch control, respectively, and δ_{ped} corresponds to the pedal input that generates a yawing moment about the body z-axis.

$$\begin{bmatrix} \Theta_1 \\ \Theta_2 \\ \Theta_3 \\ \Theta_4 \end{bmatrix} = \begin{bmatrix} +1 & -1 & +1 & +1 \\ +1 & -1 & -1 & -1 \\ +1 & +1 & -1 & +1 \\ +1 & +1 & +1 & -1 \end{bmatrix} \begin{bmatrix} \delta_{col} \\ \delta_{lat} \\ \delta_{lon} \\ \delta_{ped} \end{bmatrix} \tag{41}$$

4.2. Sizing Variables

The influence of individual design variables on key vehicle characteristics is evaluated through a comprehensive sensitivity analysis. For a fixed total aircraft weight of 9250 kg, the sizes, relative positions, and orientations of the primary vehicle components—including the rotors, wings, and horizontal tails—are initially considered as candidate design variables. Correspondingly, the vehicle characteristics of interest are selected to include total rotor power and control effectiveness about the pitch, roll, and yaw axes.

Preliminary simulation results indicate that the rotor tilt angle has a dominant influence on the required power. Consequently, it is treated as a secondary flight control means rather than a primary design variable. A trim analysis is conducted to determine the forward tilt angle that minimizes rotor power consumption over a range of flight conditions spanning hover to level forward flight up to 90 knots, as shown in Figure 5. Based on these results, a scheduled tilt-angle profile is implemented in the simulations, with the tilt angle varying smoothly between $t = 5^\circ$ and $t = 30^\circ$ to minimize power at the corresponding airspeed, as illustrated in Figure 6. In this study, the rotors are assumed to operate at the corresponding optimal tilt angle for each flight condition.

The primary design variables are selected as the rotor radius R_ω, the longitudinal separation between the front and aft rotors n, and the longitudinal and lateral rotor cant angles, denoted by i_s and i_k, respectively, as illustrated in Figure 7. For each rotor j, the longitudinal and lateral rotor incidence angles, i_{sj} and i_{kj}, are obtained by combining the rotor tilt angle $\bar{t}$ with the prescribed cant angles i_s and i_k as defined in Equation (42):

$$\begin{bmatrix} i_{s1} & i_{s2} & i_{s3} & i_{s4} \end{bmatrix} = \begin{bmatrix} -1 & +1 & +1 & -1 \end{bmatrix} i_s + \bar{t}$$
$$\begin{bmatrix} i_{k1} & i_{k2} & i_{k3} & i_{k4} \end{bmatrix} = \begin{bmatrix} +1 & +1 & -1 & -1 \end{bmatrix} i_k \tag{42}$$

In this study, σ denotes the vector of normalized design parameters listed in Table 1, while Λ represents the vector of normalized key vehicle characteristics used in the definition of the optimization objective, as summarized in Table 2. Specifically,

$$\boldsymbol{\sigma} = \begin{bmatrix} n & R_\omega & i_s & i_k \end{bmatrix}^T \qquad \boldsymbol{\Lambda} = \begin{bmatrix} \lambda_{pwr} & \lambda_{col} & \lambda_{lon} & \lambda_{lat} & \lambda_{ped} \end{bmatrix}^T \tag{43}$$

For example, the normalized vehicle characteristics λ_{pwr} with respect to the design parameter σ_i is calculated as

$$\lambda_{pwr,i}(V, \sigma_i) = \frac{P_{tot}(V, \sigma_i)}{P_{tot}(V, \sigma_i = 0)} \tag{44}$$

The sensitivity relationships between the normalized design variables σ and the normalized key vehicle characteristics $\boldsymbol{\Lambda}$ are illustrated in the matrix plot shown in Figure 8.

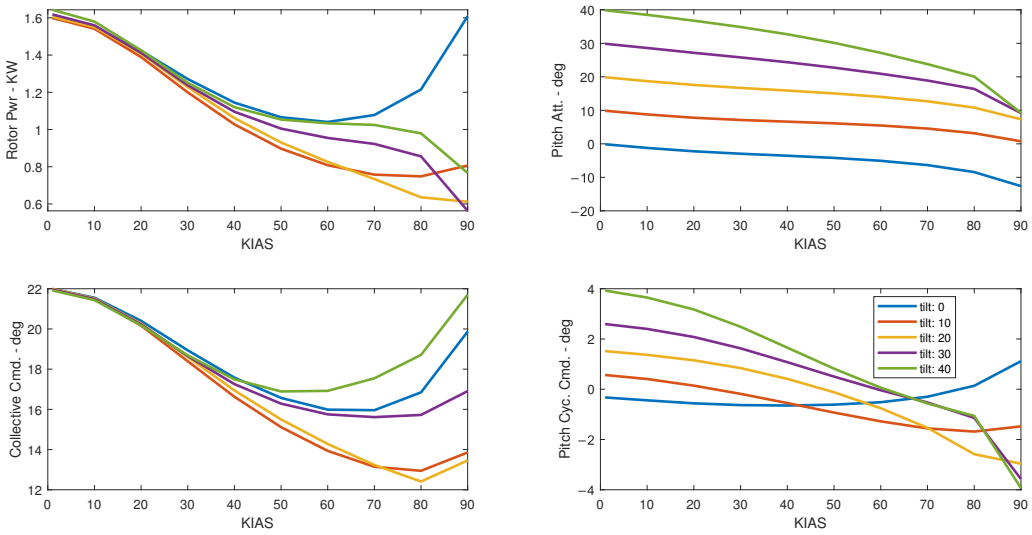


Figure 5. Trim parameters vs. airspeed for various rotor tilt angles.

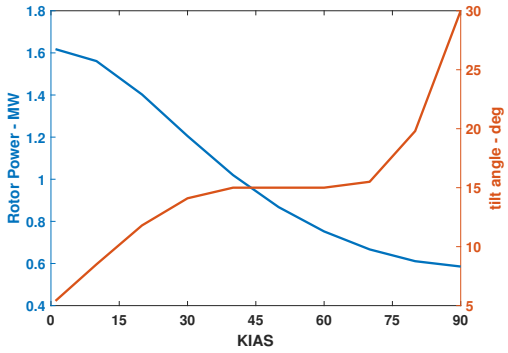


Figure 6. Minimum rotor power and optimum tilt angle vs. cruise speed.

Table 1. Limits for air vehicle design variables.

Variable	Symbol	Unit	Min	Nom	Max
Lon.Rotor Offset	n	m	9.5	11.2	12.9
Rotor Radius	R_ω	m	3.5	4.1	4.7
Lon.Cant Angle	i_s	deg	−4	0	4
Lat.Cant Angle	i_k	deg	−4	0	4
Normalized			−1	0	1

Table 2. Key vehicle characteristics.

Characteristics	Symbol	Unit	Normalized
Total Rotor Power	P_{tot}	kW	λ_{pwr}
Lon.Cyc.Control Eff.on Pitch	$M_{\delta_{lon}}$	Nm/deg	λ_{lon}
Coll.Eff.on Heave	$Z_{\delta_{coll}}$	N/deg	λ_{col}
Lat.Cyc.Control Eff.on Roll	$L_{\delta_{lat}}$	Nm/deg	λ_{lat}
Pedal Control Eff.on Yaw	$N_{\delta_{ped}}$	Nm/deg	λ_{ped}

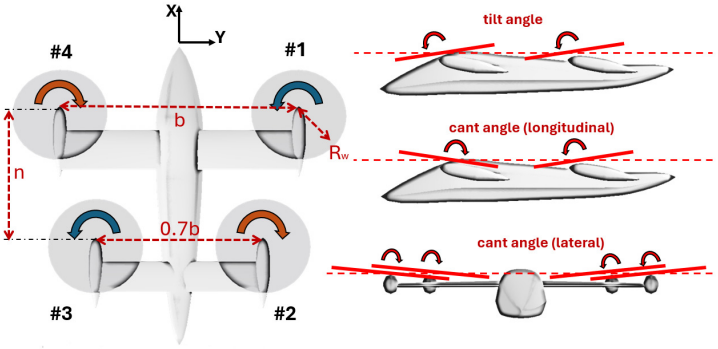


Figure 7. Air vehicle design variables.

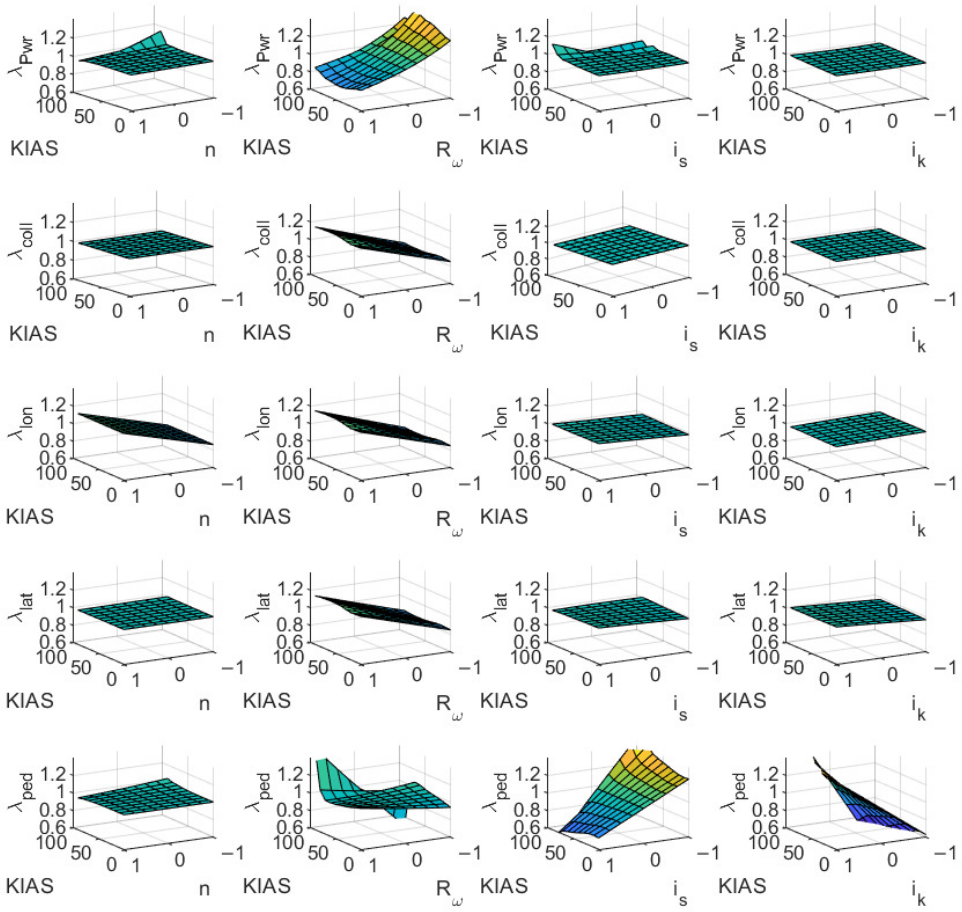


Figure 8. Sensitivity of the vehicle characteristics to design variables.

The analysis results indicate that the rotor radius has a dominant influence on the total required power, while both the rotor radius and the longitudinal separation between the rotors significantly affect pitch control effectiveness. Directional control effectiveness, on the other hand, is influenced predominantly by the longitudinal and lateral rotor cant

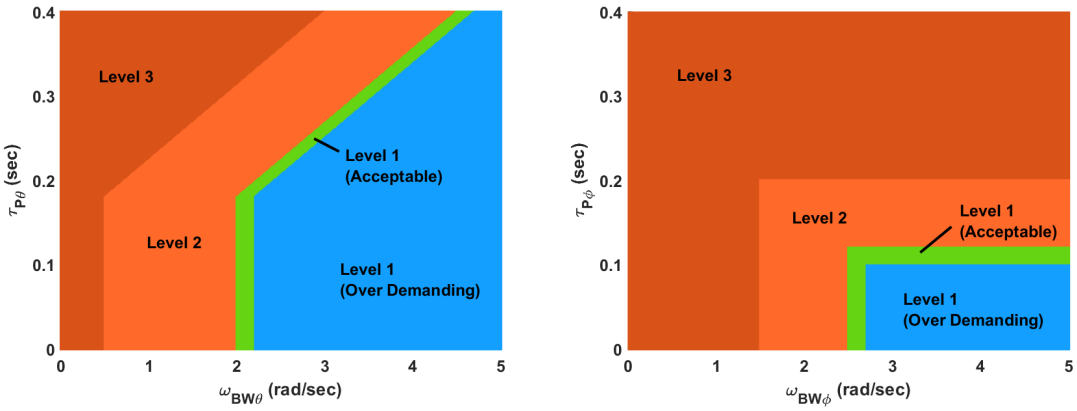
angles. The influence of rotor canting on directional control has been investigated in several previous studies, including Ref. [20].

4.3. Design Requirements and Constraints

4.3.1. Handling-Quality Requirements

The quantitative design criteria established in ADS-33 [13] constitute a well-validated framework for helicopter flight-dynamics design, providing flight-control engineers with systematic guidelines for shaping vehicle response characteristics in accordance with pilot handling-quality preferences [16]. Although these criteria were originally developed for conventional helicopters, following common practice, a subset of the ADS-33 requirements is adopted in the present study as a basis for defining representative handling-quality objectives.

Within ADS-33, small-amplitude pitch and roll attitude responses over the entire airspeed envelope are characterized for Attitude Command–Attitude Hold (ACAH) response type. The associated handling-quality requirements are defined in terms of phase delay and bandwidth, as illustrated in Figure 9. The definitions of the phase delay, τ_p, and the bandwidth, ω_{BW}, are provided in Equation (45) and further clarified in Figure 10.



(**a**) (**b**)

Figure 9. ADS-33 ACAH small-amplitude response requirements: (**a**) Pitch. (**b**) Roll.

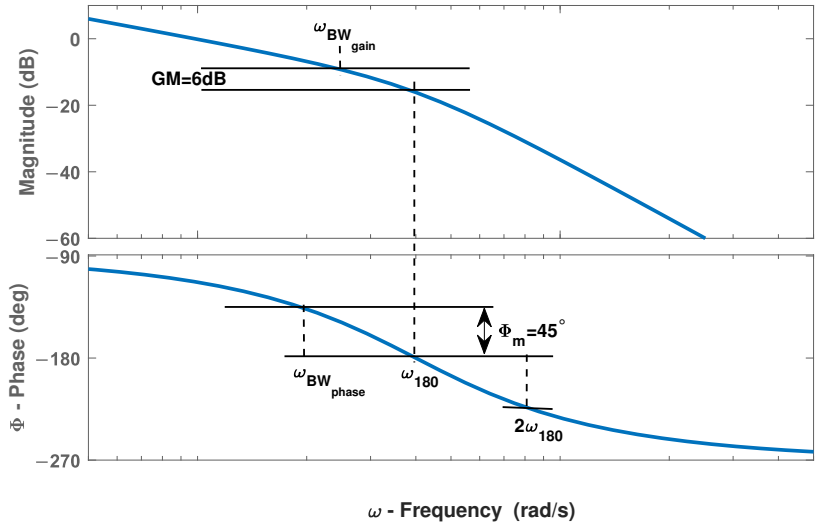


Figure 10. Bandwidth and phase delay in ADS-33.

$$\tau_p = \frac{\Delta\Phi 2\omega_{180}}{57.3(2\omega_{180})} \qquad \omega_{BW} = \omega_{BW_{phase}} \tag{45}$$

For the ACAH response type, the reference dynamics are represented by a second-order attitude model, consistent with commonly adopted formulations [21,22]. Closing the attitude-control loop within the EMF architecture shown in Figure 2 increases the overall system order. In the present application, however, the dominant slow dynamics are governed by the reference model. Accordingly, a simplified low-order equivalent representation is adopted. The closed-loop response shown in Figure 10 is therefore approximated by third-order dynamics and represented by the following transfer function:

$$\frac{X(s)}{X_i(s)} = \frac{K\omega_n^2}{s(s^2 + 2\zeta\omega_n s + \omega_n^2)} \tag{46}$$

Based on this simplified representation, an explicit relationship between the damping ratio ζ and the natural frequency ω_n is derived for an ideal (reference) closed-loop attitude-control model. This relationship aims to define the admissible set of (ζ,ω_n) combinations that satisfy Level 1 handling-quality requirements, while intentionally remaining near the Level 2 boundary to avoid overly conservative design targets.

Motivated by these considerations, the phase delay and bandwidth characteristics of the third-order system defined in Equation (46) were evaluated over a parameter grid spanning $1 \leq \omega_n \leq 10$ and $0 \leq \zeta \leq 1$. This analysis enables the ADS-33 handling-qualities boundaries, conventionally expressed in terms of bandwidth and phase delay, to be mapped onto the more familiar design parameters of natural frequency and damping ratio.

The combinations of ω_n and ζ satisfying the ADS-33 Level 1 handling-quality requirements are shown in green in Figure 11, while those corresponding to unacceptable characteristics are indicated in red. The blue region also satisfies the Level 1 requirements; however, the associated dynamics are considered excessively demanding in terms of control effort and are therefore excluded. The gray region satisfies both the phase-delay and bandwidth requirements; however, the gain-based bandwidth is lower than the phase-based bandwidth, which may increase susceptibility to pilot-induced oscillations (PIO) during precision maneuvers. Consequently, this region is also excluded from the admissible design space.

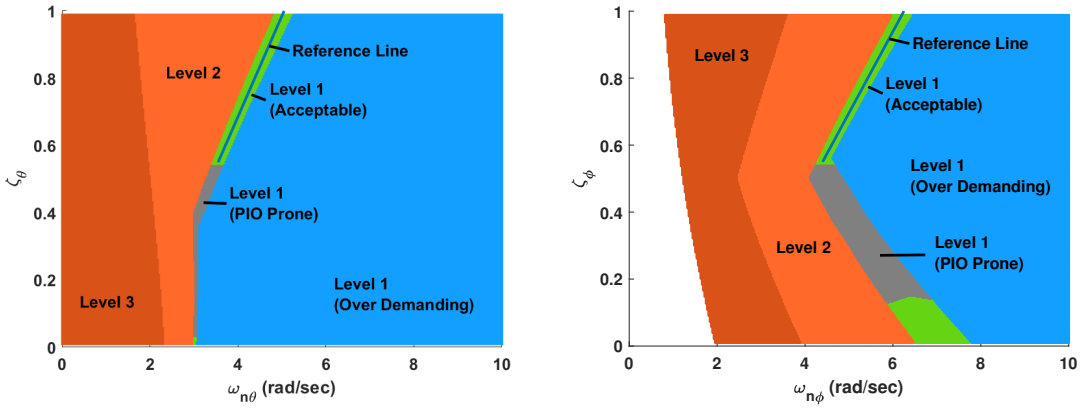


Figure 11. ADS-33 requirements mapped on ω_n-ζ grid: (**a**) Pitch. (**b**) Roll.

The regions labelled Acceptable in Figure 11 indicate that a simple functional relationship between the natural frequency ω_n and the damping ratio ζ can be identified within this domain and subsequently incorporated into the target system design. For pitch and roll attitude control, the relationship between the coefficients $-2\zeta\omega_n$ and ω_n^2 is approximated by a linear fit (see Figure 12) defined along a representative Reference Line over the intervals $3.55 \leq \omega_{n_\theta} \leq 5.05$ and $4.4 \leq \omega_{n_\phi} \leq 6.25$, yielding

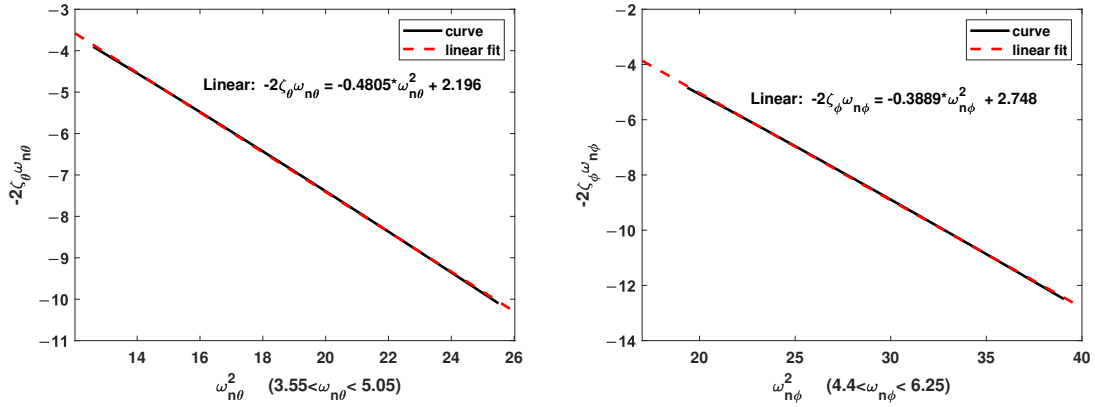
$$\begin{aligned} -2\zeta_{n_\theta}\omega_{n_\theta} &= -0.6\omega_{n_\theta}^2 + 1.03\omega_{n_\theta} \simeq -0.4805\omega_{n_\theta}^2 + 2.196 \\ -2\zeta_{n_\phi}\omega_{n_\phi} &= -0.4864\omega_{n_\phi}^2 + 1.0406\omega_{n_\phi} \simeq -0.3889\omega_{n_\phi}^2 + 2.748 \end{aligned} \tag{47}$$

Following Equations (33) and (47), and defining ν as the normalized reference-model parameter associated with ω_n^2, such that, $-1 \leq \nu \leq 1$, the reference-model state-space matrices A_m and B_m can be expressed in affine form as

$$\mathbf{A}_m = \mathbf{A}_{m0} + \mathbf{A}_{m1}\nu \qquad \mathbf{B}_m = \mathbf{B}_{m0} + \mathbf{B}_{m1}\nu \tag{48}$$

where

$$\mathbf{A}_{m0} = \mathbf{A}_m(\nu = 0) \qquad \mathbf{A}_{m1} = \frac{\partial \mathbf{A}_m}{\partial \nu} \qquad \mathbf{B}_{m0} = \mathbf{B}_m(\nu = 0) \qquad \mathbf{B}_{m1} = \frac{\partial \mathbf{B}_m}{\partial \nu} \tag{49}$$



(**a**) (**b**)

Figure 12. ADS-33 requirements fit plots: (**a**) Pitch. (**b**) Roll.

4.3.2. *D*-Stability

Let D denote a region of the complex plane that is symmetric with respect to the real axis. A real matrix $\mathbf{A} \in \mathbb{R}^{n\times n}$ is said to be D-stable if all of its eigenvalues lie in D, i.e., $\lambda_i(A) \in D, \ \ i = 1, 2, \ldots, n$. Various geometrically defined stability regions can be characterized using LMIs, including vertical strips, disks, conic sectors, or combinations thereof [17].

For a vertical strip defined by $D = \{x + jy \mid -\beta < x < -\alpha < 0\}$, the matrix $\mathbf{A}$ is D-stable if and only if there exists a symmetric positive definite matrix $\mathbf{P}$ such that

$$\begin{aligned} \mathbf{P} &> 0, \\ \mathbf{A}^T\mathbf{P} + \mathbf{P}\mathbf{A} + 2\alpha\mathbf{P} &< 0, \\ \mathbf{A}^T\mathbf{P} + \mathbf{P}\mathbf{A} + 2\beta\mathbf{P} &> 0. \end{aligned} \tag{50}$$

Similarly, for a disk of radius r centered at $-q + j0$, defined as $D = \{x + jy \mid (x + q)^2 + y^2 < r^2\}$, the matrix $\mathbf{A}$ is D-stable if and only if there exists a symmetric positive definite matrix $\mathbf{P}$ satisfying

$$\begin{aligned} \mathbf{P} &> 0, \\ \begin{bmatrix} -r\mathbf{P} & q\mathbf{P} + \mathbf{A}\mathbf{P} \\ q\mathbf{P} + \mathbf{P}\mathbf{A}^T & -r\mathbf{P} \end{bmatrix} &< 0. \end{aligned} \tag{51}$$

In this study, a composite region formed by the intersection of a vertical strip and a disk is employed.

4.3.3. Maneuverability Requirements

Maneuverability requirements typically impose a lower bound on system gain to ensure a minimum level of amplification in response to command inputs. For an open-loop system described by the input–output relation $\mathbf{y} = G(\mathbf{u})$, such a requirement can be stated as follows: given a maximum allowable control input $\mathbf{u}_{max}$, the corresponding steady-state output must exceed a prescribed minimum value $\mathbf{y}_{min}$. A comprehensive treatment of maneuverability requirement formulations in terms of LMIs, including open- and closed-loop representations for both static and dynamic systems, is provided in Ref. [23]. In the present study, only open-loop maneuverability requirements are considered. Consider a generic open-loop system governed by

$$\begin{aligned} \dot{\mathbf{x}} &= \mathbf{A}\mathbf{x} + \mathbf{B}_1\mathbf{u} \\ \mathbf{y} &= \mathbf{C}\mathbf{x} \end{aligned} \tag{52}$$

where $\mathbf{x}$, $\mathbf{u}$ and $\mathbf{y}$ denote the state, input, and output vectors, respectively. Let subscripts i and j denote the ith output and jth input channels. The transfer function form u_j to y_i is given by

$$y_i(s) = \left(\left[\mathbf{C}(s\mathbf{I} - \mathbf{A})^{-1}\mathbf{B}_1 \right]_{i,j} \right) u_j(s) \tag{53}$$

Assuming $\mathbf{C} = \mathbf{I}$ and that all states except x_i remain at their equilibrium values, the steady-state relationship between x_i and u_j reduces to

$$\begin{aligned} 0 &= \mathbf{A}_{i,i}x_i + \mathbf{B}_{1\,i,j}u_j \\ y_i &= x_i \end{aligned} \tag{54}$$

Under these assumptions, an open-loop maneuverability constraint can be expressed as the inequality

$$\mathbf{A}_{(i,i)}x_{imin} + \mathbf{B}_{1(i,j)}u_{j_{max}} < 0 \tag{55}$$

which guarantees that the required minimum steady-state output (or state) response x_{imin} is achievable under the maximum allowable control input $u_{j_{max}}$.

5. Results

The results obtained from the implementation of the proposed iterative procedure in VTOL air vehicle sizing problem are presented for three distinct problem cases. These results include the converged values of the design variables, the corresponding gains of the EMF controller, the convergence behavior of the algorithm, and the closed-loop time-history responses for selected maneuvering scenarios. The time-domain responses compare the initial condition—corresponding to the first half iteration in which the controller gains are synthesized with fixed design variables—with the final condition associated with the converged design variables and controller gains.

The proposed algorithm is implemented in MATLAB using the YALMIP toolbox [24] to solve the resulting LMI optimization problems. Unless otherwise stated, the normalized plant and reference-model design parameters are constrained as $-1.0 \leq \sigma_i \leq 1.0$ and $-1.0 \leq \nu_j \leq 1.0$, respectively. The iterative optimization procedure is terminated when the prescribed convergence criteria are satisfied; otherwise, a maximum of ten iterations is performed.

The attitude dynamics is parameterized according to Equation (47) and incorporated directly into the optimization framework through the reference-model parameters defined in Equation (48), which are selected to satisfy the ADS-33 handling-quality requirements.

The plant and reference-model outputs are selected as the vertical velocity and pitch attitude for the longitudinal cases, and as the roll attitude and lateral velocity for the lateral-directional cases; accordingly, the output matrix $\mathbf{H}$ is defined to reflect these selections.

Longitudinal:

$$\mathbf{y} = \mathbf{H}\mathbf{x} = \begin{bmatrix} w & \theta \end{bmatrix}^T \qquad \mathbf{y}_m = \mathbf{H}\mathbf{x}_m = \begin{bmatrix} w_m & \theta_m \end{bmatrix}^T \qquad \mathbf{H} = \begin{bmatrix} 0 & 1 & 0 & 0 \\ 0 & 0 & 0 & 1 \end{bmatrix}$$

Lateral:

$$\mathbf{y} = \mathbf{H}\mathbf{x} = \begin{bmatrix} \phi & v \end{bmatrix}^T \qquad \mathbf{y}_m = \mathbf{H}\mathbf{x}_m = \begin{bmatrix} \phi_m & v_m \end{bmatrix}^T \qquad \mathbf{H} = \begin{bmatrix} 0 & 0 & 1 & 0 \\ 1 & 0 & 0 & 0 \end{bmatrix}$$

In all cases the diagonal weighting matrix $\mathbf{L}$ is defined as

$$\mathbf{L} = \begin{bmatrix} 1 & 0 \\ 0 & 5 \end{bmatrix}$$

In all problem formulations, D-stability constraints are enforced to ensure that the closed-loop poles lie within the real interval $[-12, \ -0.5]$ and, in addition, remain inside a disk of radius 9 centered at -10 on the real axis, as defined by Equations (50) and (51).

5.1. Case #1: Optimize Directional Control Effectiveness Using H_∞ Synthesis

In the first case, the objective is to improve the directional control effectiveness, λ_{ped}, with respect to the longitudinal and lateral cant angles, i_s and i_k, under the 60 kts cruise condition. The optimization is carried out using an H_∞-based synthesis formulation. The cost function is defined as

$$C_{\#1} = 0.61 i_s - 0.39 i_k$$

The open-loop system matrices defined by the linear parametric model in Equation (32) are obtained by linearizing the nonlinear aircraft model about the selected trim condition. The resulting nominal and sensitivity matrices for the lateral-directional dynamics at 60 kts cruise condition are presented in Equation (A2). The parametric reference-model matrices defined in Equation (33) are obtained using the procedure described previously and expressed in the affine form of Equation (47), as given in Equation (A4).

The convergence history of the iterative procedure, together with the feasibility status of the original BMI constraint $\Delta\mathbf{T}$, is presented in Figure 13. The corresponding optimized plant parameters and controller gains are summarized below.

$$\mathbf{K}_{p_{\#1}} = \begin{bmatrix} 0.5998 & 0.3508 & 1.6776 & -0.6616 \\ -0.3513 & -0.2660 & -2.2037 & -0.2579 \end{bmatrix}$$

$$\mathbf{K}_{m_{\#1}} = \begin{bmatrix} -0.5017 & -0.0958 & -1.1524 & 0.0000 \\ 0.3415 & 0.1482 & 1.7797 & -0.0000 \end{bmatrix}$$

$$\mathbf{K}_{e_{\#1}} = \begin{bmatrix} -3.3788 & -3.9091 \\ 5.2368 & 2.7264 \end{bmatrix} \qquad \boldsymbol{\sigma}_{\#1} = \begin{bmatrix} -1.0 & 1.0 \end{bmatrix}^T \qquad \boldsymbol{\nu}_{\#1} = \begin{bmatrix} 0.6998 \end{bmatrix}$$

The optimized design converges to the lower and upper bounds of cant-angle variables, indicating that increased cant configuration significantly enhances directional control effectiveness under the selected operating condition.

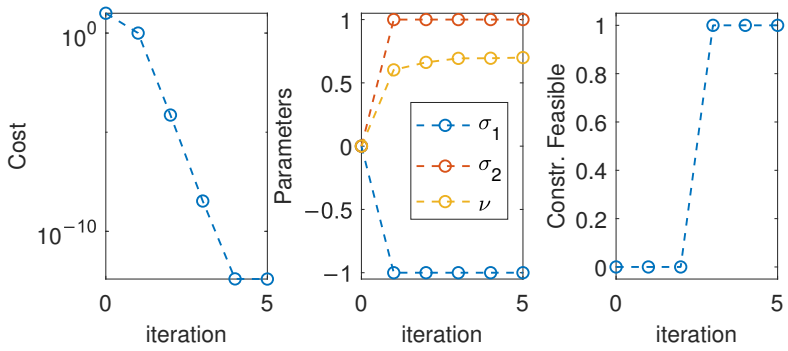


Figure 13. Convergence history: Case#1.

The change in aircraft control effort for Case#1, from the initial controller synthesis with fixed plant variables to the final co-designed plant–controller configuration, is summarized in Table 3.

Table 3. Change in design objectives (initial controller synthesis with fixed plant variables vs. final co-designed plant and controller): Case#1.

Parameter	Unit	Trim	Initial	Final	Change (%)
Max. lateral cyclic command	deg	0	−6.39	−2.10	−67
Max. pedal command	deg	0	15.10	3.88	−74
Max. rotor 1 command	deg	11.75	33.19	17.69	−72
Max. rotor 2 command	deg	14.88	6.03	12.81	−77
Max. rotor 3 command	deg	14.87	23.73	16.95	−77
Max. rotor 4 command	deg	11.78	−9.65	5.84	−72
Max. rotor 1 command rate	deg/s	0	603	174	−71
Max. rotor 2 command rate	deg/s	0	−215	−37	−83
Max. rotor 3 command rate	deg/s	0	215	37	−83
Max. rotor 4 command rate	deg/s	0	−603	−174	−71

The time histories of the control inputs, system states, and actuator responses are presented in Figures 14 and 15.

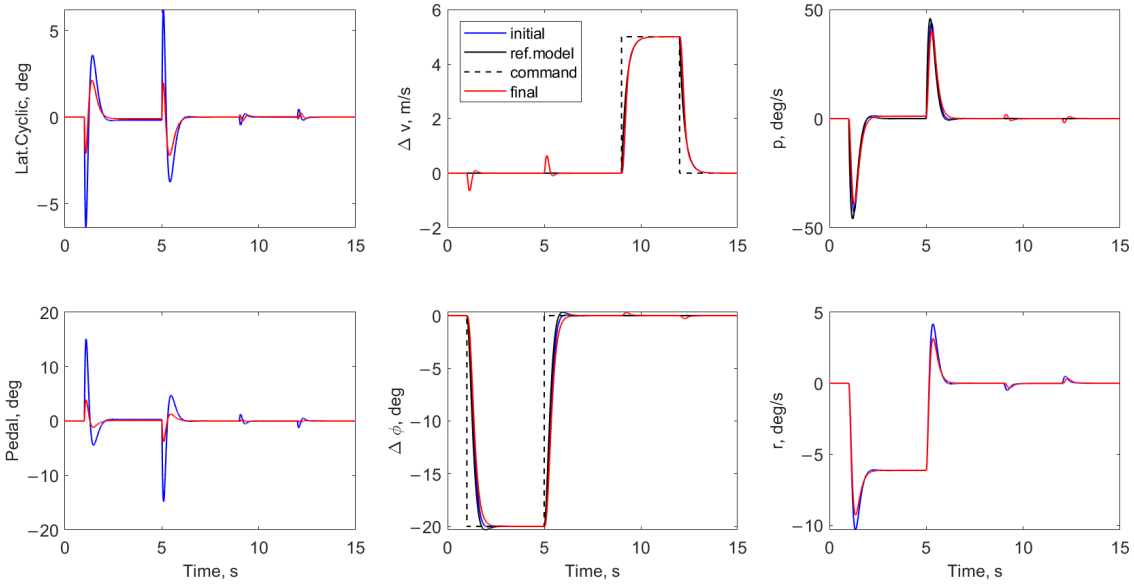


Figure 14. Time history plots for Case #1: controls and states.

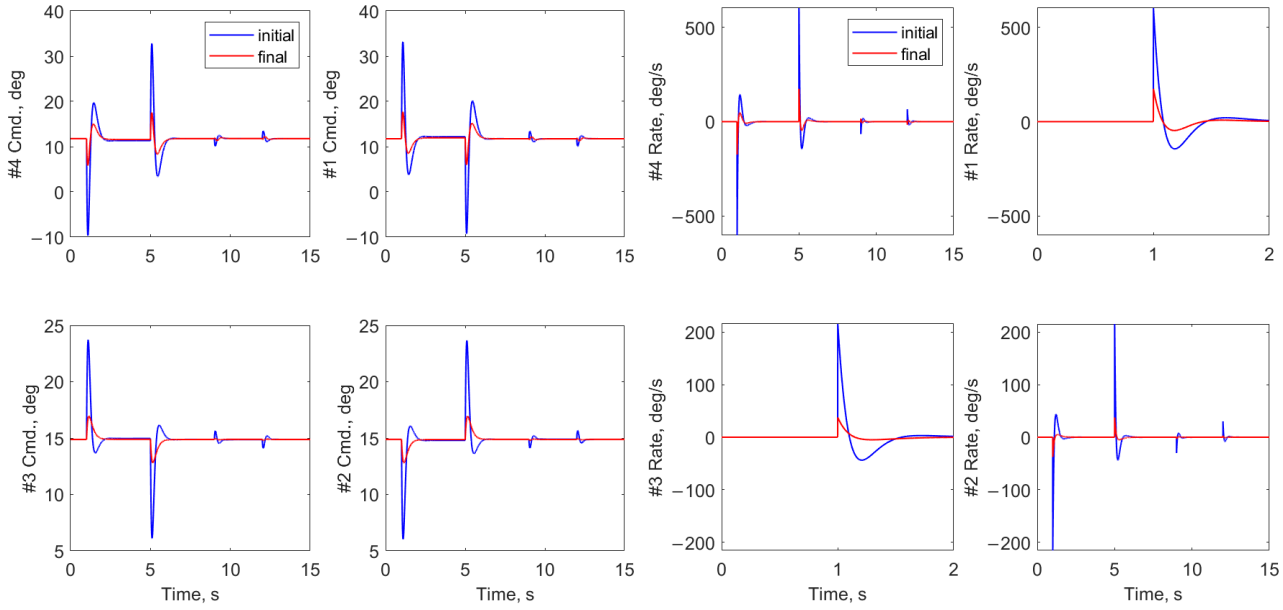


Figure 15. Time history plots for Case #1: (**a**) Actuator commands. (**b**) Actuator rates.

Comparison Between the Affine Plant Model and the Modified Plant Model

The analyses in this study are conducted using an affine plant model obtained by trimming, linearizing, and parameterizing the system about the initial design configuration. This formulation assumes that the variations in the plant dynamics with respect to the design parameters can be adequately represented by a linear approximation. To assess the validity of this assumption and its influence on the results, the affine-model predictions are compared with those obtained from a plant model retrimmed and relinearized at the converged design parameters.

The linear state-space matrices **A** and **B** obtained from the affine approximation and the retrimmed and relinearized plant models are presented below.

$$\mathbf{A}_{aff.} = \begin{bmatrix} -0.0582 & 5.4796 & 9.6470 & -30.6077 \\ -0.4667 & 7.7801 & 0.0000 & -0.3964 \\ 0 & 1.0000 & 0 & 0.1728 \\ 0.0120 & 0.0672 & 0.0000 & -0.1897 \end{bmatrix} \quad \mathbf{B}_{aff.} = \begin{bmatrix} 5.7266 & 0.0076 \\ 195.3291 & 70.8829 \\ 0 & 0 \\ -4.8720 & -14.6114 \end{bmatrix}$$

$$\mathbf{A}_{retr.} = \begin{bmatrix} -0.0619 & 5.2524 & 9.6697 & -30.5599 \\ -0.1593 & 8.1960 & 0 & -0.4605 \\ 0 & 1.0000 & 0 & 0.1688 \\ -0.0084 & 0.0056 & 0 & -0.1435 \end{bmatrix} \quad \mathbf{B}_{retr.} = \begin{bmatrix} 2.7739 & -0.0327 \\ 189.6893 & 70.2329 \\ 0 & 0 \\ -4.3917 & -9.8583 \end{bmatrix}$$

The corresponding time-domain responses of the two plant models are compared in Figure 16. The figure shows that, despite the substantial variation in the geometric design parameters, the performance degradation observed with the retrimmed plant model, while not negligible, remains relatively limited compared with the affine-model prediction.

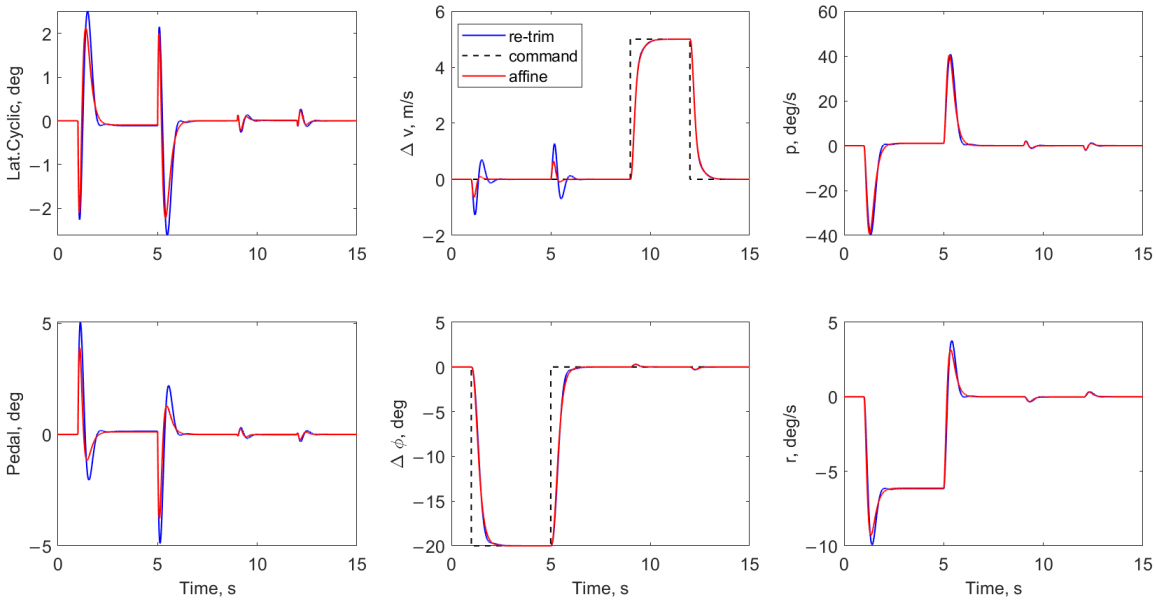


Figure 16. Time history plots for the two plant models: controls and states.

5.2. Case #2: Effect of Reference Model Parameter ν in Optimization

In Case #1, the design parameters are constrained within the bounds $-1 \leq \sigma \leq 1$ and $-1 \leq \nu \leq 1$. To assess the influence of the reference-model parameter ν on the optimization process, two complementary cases are considered.

5.2.1. Effect of ν with Fixed Plant-Design Parameters ($\sigma = 0$)

In the first sub-case, the effect of optimizing only the reference-model parameter ν is investigated, while the air-vehicle design parameters are fixed at $\sigma = 0$. The convergence history of the iterative procedure is illustrated in Figure 17, while the closed-loop time-history responses of the system states and control inputs are presented in Figure 18. The corresponding variations in key control-effort metrics, including the maximum lateral cyclic and pedal commands, are summarized in Table 4.

The corresponding variations in bandwidth and phase delay for the roll attitude control loop are summarized in Table 5. In addition, the effects of the parameter ν on the bandwidth and phase delay are illustrated through a parameter sweep in Figure 19.

Table 4. Effect of ν with fixed plant-design parameters ($\sigma = 0$).

Parameter	Unit	Trim	Initial	Final	Change (%)
Max. lateral cyclic command	deg	0	−6.39	−6.22	−2.7
Max. pedal command	deg	0	15.1	14.66	−2.9
Max. rotor 1 command	deg	11.74	33.19	32.58	−2.8
Max. rotor 2 command	deg	14.88	6.03	6.31	−3.2
Max. rotor 3 command	deg	14.87	23.73	23.45	−3.2
Max. rotor 4 command	deg	11.78	−9.67	−9.06	−2.8
Max. rotor 1 command rate	deg/s	0	603	599	−0.7
Max. rotor 2 command rate	deg/s	0	−215	−214	−0.5
Max. rotor 3 command rate	deg/s	0	215	214	−0.5
Max. rotor 4 command rate	deg/s	0	−603	−599	−0.7

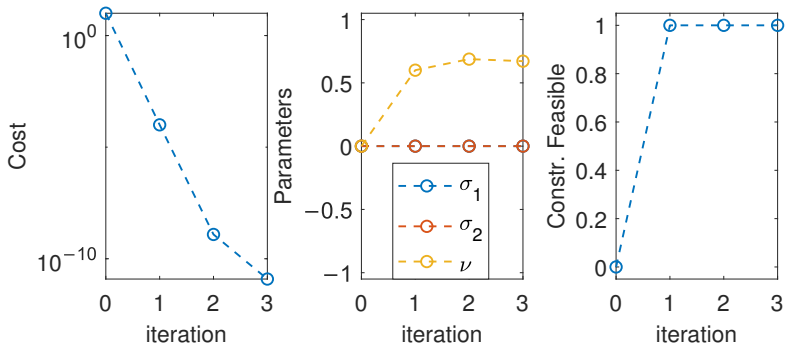


Figure 17. Convergence history.

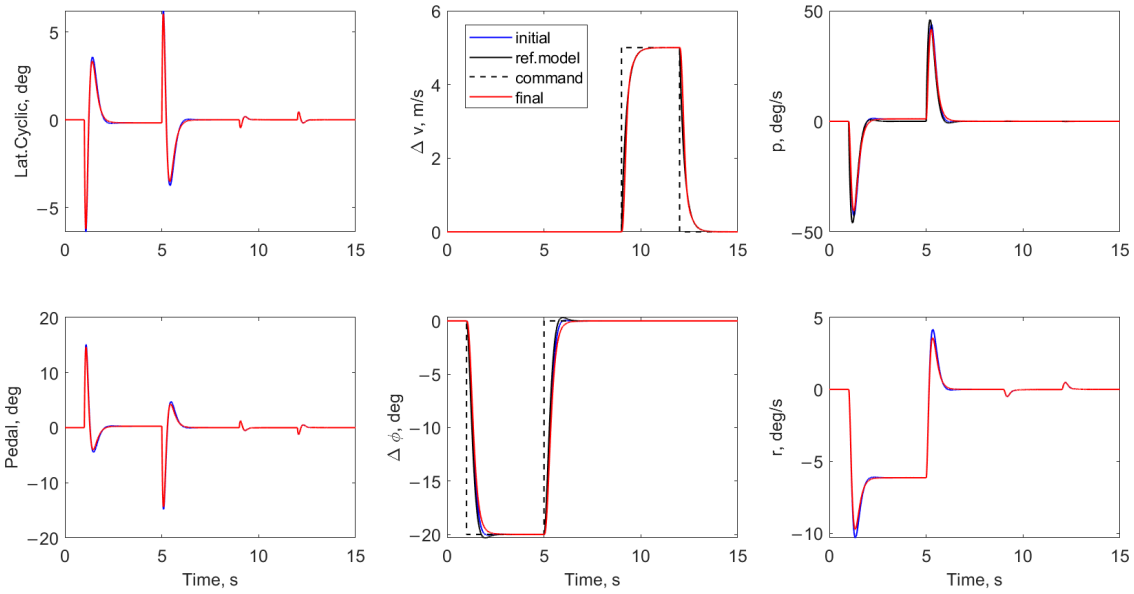


Figure 18. Time history plots—the effect of ν with $\sigma = 0$ fixed: controls and states.

Table 5. Change in bandwidth and phase delay with fixed plant-design parameters ($\sigma = 0$).

Parameter	Unit	Initial	Final	Change (%)
ν	-	0.0	0.67	-
Bandwidth	rad/s	3.55	3.41	−3.9
Phase delay	s	0.086	0.083	−3.5

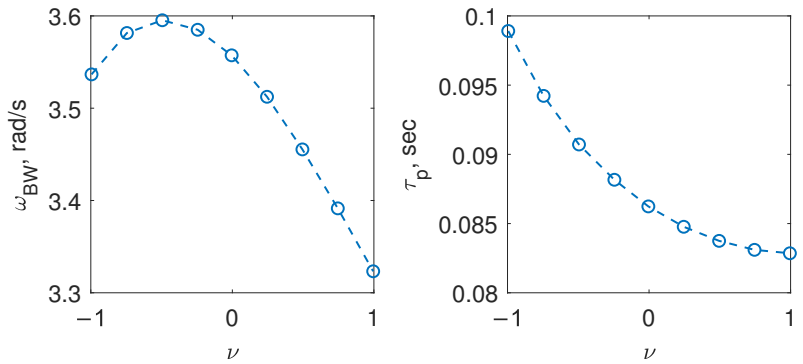


Figure 19. Change of bandwidth and phase delay for ν sweep.

5.2.2. Effect of ν with Optimized Plant-Design Parameters (σ Free)

In the second sub-case, the influence of ν is examined when the plant-design parameters are also included in the optimization. Specifically, the results are compared for two scenarios: (a) ν fixed and (b) ν treated as an additional design variable, while σ is allowed to vary within the bounds $-1 \leq \sigma \leq 1$ in both cases. The resulting time-domain responses after optimization are compared in Figure 20, and the corresponding changes in the control-effort metrics are summarized in Table 6.

Table 6. Effect of ν with optimized plant-design parameters (σ free).

Parameter	Unit	Trim	ν Fixed	ν Free	Change (%)
Max. lateral cyclic command	deg	0	−2.17	−2.11	−2.8
Max. pedal command	deg	0	4.03	3.89	−3.5
Max. rotor 1 command	deg	11.74	17.89	17.7	−3.1
Max. rotor 2 command	deg	14.88	12.7	12.81	−5.0
Max. rotor 3 command	deg	14.87	17.06	16.94	−5.5
Max. rotor 4 command	deg	11.78	5.63	5.83	−3.3
Max. rotor 1 command rate	deg/s	0	175	174	−0.6
Max. rotor 2 command rate	deg/s	0	−37.77	−37.56	−0.6
Max. rotor 3 command rate	deg/s	0	37.77	37.56	−0.6
Max. rotor 4 command rate	deg/s	0	−175	−174	−0.6

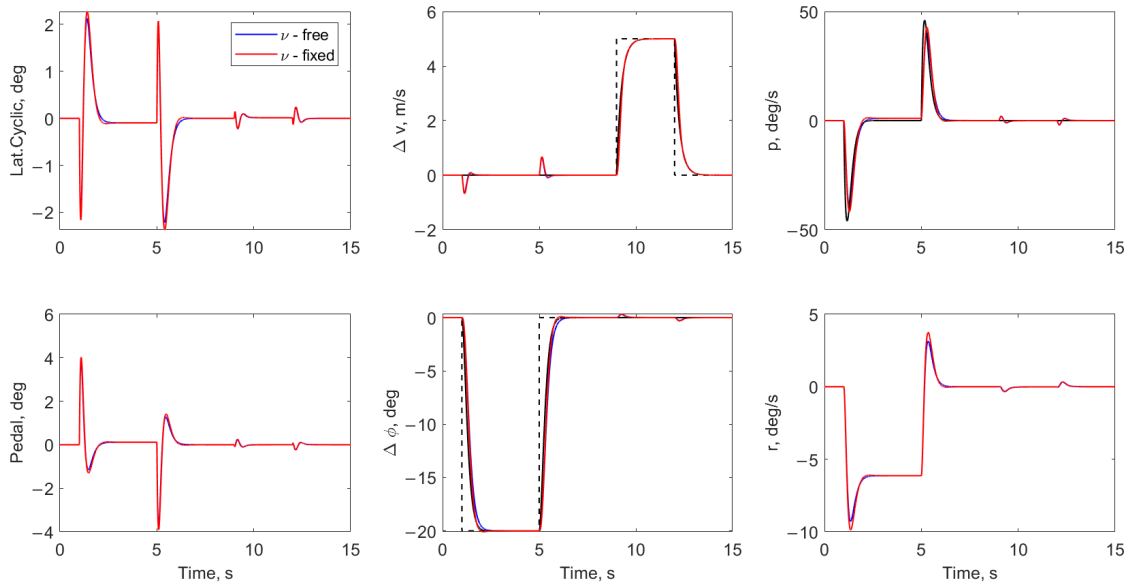


Figure 20. Time history plots—The effect of ν with σ free: controls and states.

The corresponding variations in bandwidth and phase delay for the roll attitude control loop are summarized in Table 7.

Table 7. Change in bandwidth and phase delay with free plant-design parameters.

Parameter	Unit	ν Fixed	ν Free	Change (%)
ν	-	0.0	0.70	-
Bandwidth	rad/s	3.32	3.15	−5.1
Phase delay	s	0.095	0.091	−4.5

Both subproblems of Case #2 exhibit an improvement of approximately 3–5% in control-actuation demand when the reference-model parameter ν is included in the opti-

mization, whereas the corresponding reduction in actuator-rate demand is considerably smaller. For the attitude-control loop, both the bandwidth and phase delay remain within the Level 1 boundaries and lie close to the Acceptable region defined in Figure 9. Both metrics decrease relative to the baseline case. The parameter sweep presented in Figure 19 indicates that the bandwidth reaches a maximum near $\nu = -0.5$, whereas the phase delay attains its minimum near $\nu = 1.0$.

5.3. Case #3: Optimization of Required Power and Rotor Offset with Pitch-Rate Constraint

In Case #3, the objective is to minimize the longitudinal rotor offset while maintaining a minimum level of pitch control effectiveness. The optimization is performed at the 60 kts cruise condition, with the first design parameter constrained to satisfy $-0.9 \leq \sigma_1 \leq 1$.

Specifically, a minimum pitch rate of, $q_{min} = 20^\circ/\text{s}$, must be achieved under a maximum longitudinal cyclic deflection of $\delta_{lon\,max} = 1^\circ$. This requirement is enforced through the following inequality constraint:

$$\left(\mathbf{A}_{03,3} + \mathbf{A}_{13,3}\sigma_1 + \mathbf{A}_{23,3}\sigma_2\right)q_{min} + \left(\mathbf{B}_{03,2} + \mathbf{B}_{13,2}\sigma_1 + \mathbf{B}_{23,2}\sigma_2\right)\delta_{lon\,max} \geq 0$$

where $(\cdot)_{j,k}$ denotes the (j,k)th element of the corresponding matrix. The cost function for this case, derived from the sensitivity analysis, is defined as

$$C_{\#3} = 0.15n - 0.85R_\omega$$

The nominal and sensitivity matrices associated with the longitudinal dynamics at 60 kts cruise condition are given in Equation (A1). The parametric reference-model matrices defined in Equation (33) are obtained following the procedure described previously and expressed in the affine form of Equation (47) as shown in Equation (A3).

The resulting optimized plant parameters and controller gains are given by

$$\mathbf{K}_{p_{\#3}} = \begin{bmatrix} 0.0062 & -0.2894 & -0.6638 & 0.1137 \\ 0.3220 & 0.0465 & 0.6915 & 10.0136 \end{bmatrix}$$

$$\mathbf{K}_{m_{\#3}} = \begin{bmatrix} -0.0000 & 0.2310 & -0.0049 & -0.0815 \\ -0.0000 & 0.0124 & -0.6623 & -10.6359 \end{bmatrix}$$

$$\mathbf{K}_{e_{\#3}} = \begin{bmatrix} 0.6853 & -0.5688 \\ 0.1183 & -73.4031 \end{bmatrix} \qquad \boldsymbol{\sigma}_{\#3} = \begin{bmatrix} -0.9 & 0.5774 \end{bmatrix}^T \qquad \boldsymbol{\nu}_{\#3} = \begin{bmatrix} 0.7398 \end{bmatrix}$$

The convergence history of the optimization process, together with the feasibility status of the original BMI constraint $\Delta\mathbf{T}$, is presented in Figure 21, while the corresponding changes in the design objectives are summarized in Table 8.

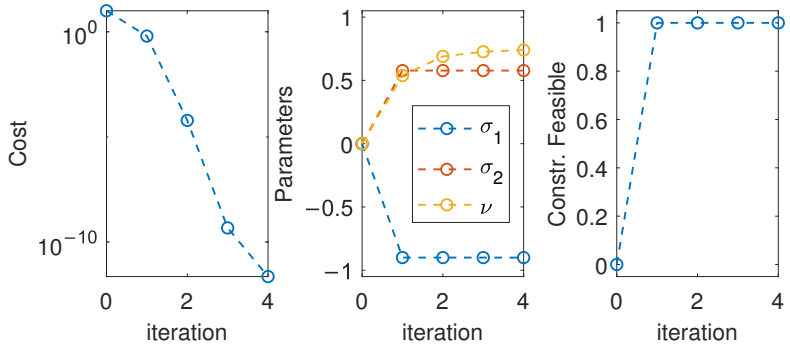


Figure 21. Convergence history: Case #3.

Table 8. Change in design objectives (initial controller synthesis with fixed plant variables vs. final co-designed plant and controller)—Case #3.

Parameter	Unit	Initial	Final	Change (%)
Available power	kW	742.6	751.4	+1.2
Max. collective command	deg	−1.16	−1.09	−6.0

The time histories of the control inputs, system states, and actuator responses are presented in Figures 22 and 23.

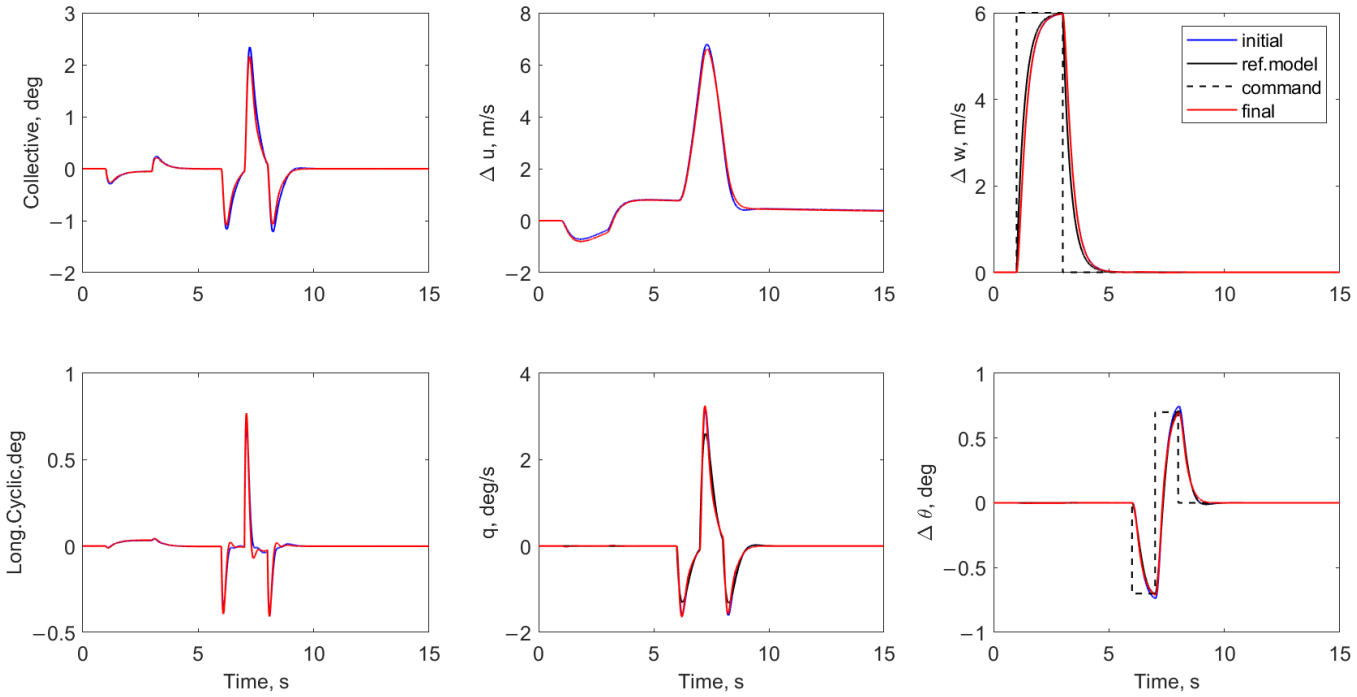
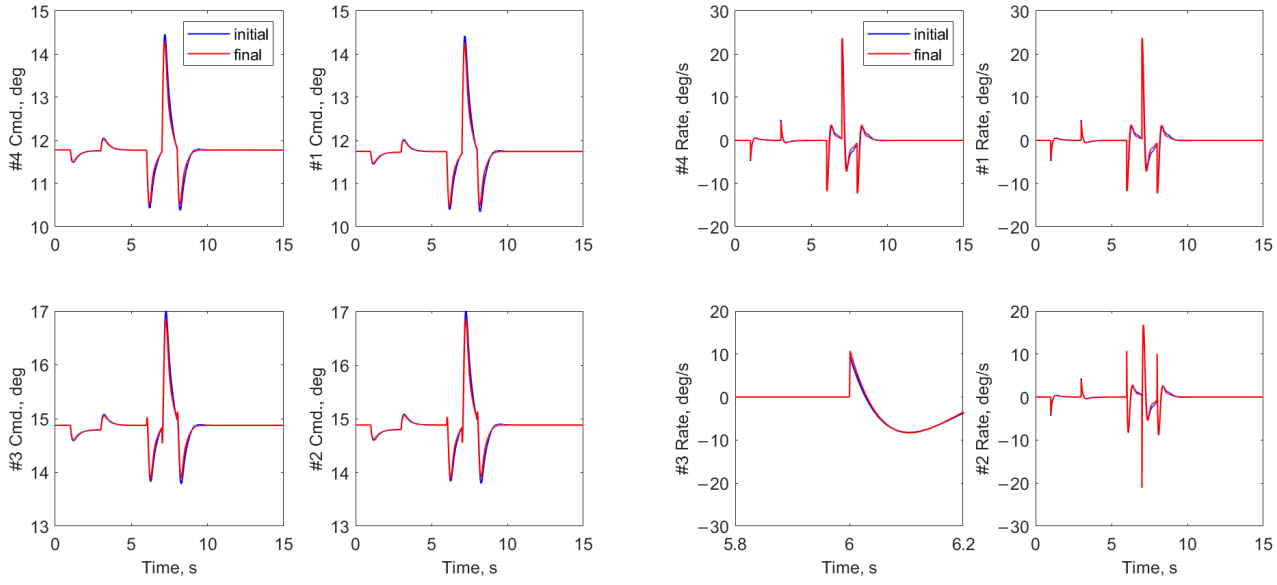


Figure 22. Time history plots for Case #3: controls and states.



(**a**) (**b**)

Figure 23. Time history plots for Case #3: (**a**) Actuator commands. (**b**) Actuator rates.

The results indicate that the optimized configuration converges toward the lower bound of the first parameter, accompanied by an increase in the second parameter. The active constraints are the pitch-rate constraint and the lower bound of the first parameter. This behavior reflects the inherent trade-off between increasing the rotor radius and reducing the longitudinal rotor offset while satisfying the prescribed minimum pitch-control-effectiveness constraint. As a consequence of this trade-off, the optimized configuration exhibits a slight increase in total rotor power, together with a reduction in the overall control power, consistent with the changes in rotor offset and the imposed minimum control-effectiveness requirement.

6. Discussion

This study presented a general iterative LMI-based co-design methodology for the integrated optimization of plant parameters, controller gains, and reference-model dynamics within an Explicit Model Following framework. In contrast to conventional model-following approaches, where the reference model is prescribed a priori, the proposed formulation parameterizes the reference-model dynamics and includes the associated parameters directly in the optimization. This introduces an additional degree of freedom for balancing plant design and control-system performance while maintaining the prescribed closed-loop response characteristics. The framework was developed for H_2, H_∞, and mixed H_2/H_∞ state-feedback synthesis, thereby extending the applicability of the previously developed LQR-based co-design approach. Its effectiveness is demonstrated through a VTOL aircraft application, in which the reference-model dynamics are defined in accordance with ADS-33 handling-quality requirements.

The bilinearities arising from the simultaneous dependence of the closed-loop conditions on the controller, plant-design, and reference-model parameters were addressed through a perturbation-based formulation. The resulting BMI-constrained problem was decomposed into sequential LMI subproblems, enabling the design variables and controller gains to be updated iteratively using standard convex optimization tools. The methodology is demonstrated on a representative VTOL air-vehicle sizing problem subject to closed-loop stability, ADS-33-based handling-qualities, and maneuverability constraints.

The VTOL case studies demonstrated the capability of the proposed framework to accommodate different and competing design objectives. Optimization of the rotor cant angles produced substantial improvements in directional control effectiveness and associated control demand. The investigation of reference-model parametrization further showed that allowing the reference-model parameter ν to vary yields an additional improvement of approximately 3–5% when the plant parameters are optimized simultaneously. This gain is modest compared with the substantially larger 50–70% improvement achieved through plant–controller co-design, as measured by comparing the initial controller synthesis with fixed plant variables against the final co-designed plant and controller. Although comparatively modest, this additional improvement demonstrates that the prescribed target dynamics influence the resulting integrated optimum and should therefore not necessarily be treated as fixed quantities. The longitudinal design case further demonstrated the trade-off between rotor radius and longitudinal rotor offset while satisfying the imposed pitch-control-effectiveness constraint.

Overall, the results demonstrate the feasibility of incorporating parametric reference-model dynamics directly into an LMI-based plant–controller co-design framework. The proposed methodology provides a systematic framework for simultaneously addressing vehicle sizing, control-system performance, stability, controllability, and handling-qualities requirements within the integrated design process. Future work should examine the influence of reference-model parametrization in greater detail to better understand how

the prescribed target dynamics affect the integrated co-design optimum. A systematic comparison with alternative co-design approaches would also be valuable. In addition, extending the methodology to higher-fidelity vehicle models, multiple operating conditions, a broader set of design variables, and more comprehensive handling-quality and performance requirements would help assess its robustness and applicability to more complex design problems.

Author Contributions: Conceptualization, E.H.O.; methodology, E.H.O.; software, E.H.O.; validation, E.H.O.; formal analysis, E.H.O.; investigation, E.H.O.; resources, E.H.O.; data curation, E.H.O.; writing—original draft preparation, E.H.O.; writing—review and editing, O.T.; visualization, E.H.O.; supervision, O.T.; project administration, O.T. All authors have read and agreed to the published version of the manuscript.

Funding: This research received no external funding.

Data Availability Statement: The original contributions presented in this study are included in the article. Further inquiries can be directed to the corresponding author.

Conflicts of Interest: The authors declare no conflicts of interest.

Nomenclature

C	Cost
i_s, i_k	Rotor cant angle—longitudinal, lateral
L, M, N	Moment in body roll, pitch, yaw axes
n	Offset between fore and aft rotors
p, q, r	Roll, pitch, yaw rate
P_{tot}	Total rotor power
R_ω	Rotor radius
S_w	Wing area
t	Rotor tilt angle
u, v, w	Longitudinal, lateral, vertical speed in body axes
V	Speed
w	Weighting coefficient
$\mathbf{x}$	System states
X, Y, Z	Force in body x, y, z axes
$\boldsymbol{\delta}, \mathbf{u}$	System inputs
Δ	Difference, e.g., from trim conditions
ζ	Damping coefficient
$\boldsymbol{\eta}, \mathbf{w}$	External disturbance—reference inputs
θ	Pitch attitude
Θ	Blade pitch command
ϕ	Roll attitude
σ	Plant-design parameter vector
τ	Time constant
τ_p	Phase delay
ω	Frequency
ω_{BW}	Bandwidth frequency
$*$	Transpose of the symmetric element in a matrix

Appendix A

The nominal system matrices and sensitivity matrices associated with the VTOL aircraft dynamics at 60 kts cruise condition.

Appendix A.1. Longitudinal

$$\mathbf{A}_0^{60,\text{lon}} = \begin{bmatrix} -0.0037 & 0.1225 & -5.2571 & -9.6526 \\ -0.1593 & -0.3483 & 29.4920 & -1.7306 \\ 0.1107 & -0.2097 & -2.2862 & 0 \\ 0 & 0 & 1.0000 & 0 \end{bmatrix} \quad \mathbf{B}_0^{60,\text{lon}} = \begin{bmatrix} 6.8822 & 0.3354 \\ -39.9978 & 0.2125 \\ -1.4968 & 38.0329 \\ 0 & 0 \end{bmatrix}$$

$$\mathbf{A}_1^{60,\text{lon}} = \begin{bmatrix} 0.0001 & -0.0001 & -0.0056 & 0 \\ 0 & -0.0001 & -0.0010 & 0 \\ -0.0002 & 0 & -0.7623 & 0 \\ 0 & 0 & 0 & 0 \end{bmatrix} \quad \mathbf{B}_1^{60,\text{lon}} = \begin{bmatrix} -0.0003 & -0.0481 \\ 0.0012 & -0.0305 \\ -0.0014 & 5.7338 \\ 0 & 0 \end{bmatrix} \tag{A1}$$

$$\mathbf{A}_2^{60,\text{lon}} = \begin{bmatrix} -0.0016 & 0.0242 & -0.4056 & 0.0254 \\ 0.0277 & -0.0897 & -0.0979 & -0.1419 \\ -0.0007 & -0.0046 & -0.4120 & 0 \\ 0 & 0 & 0 & 0 \end{bmatrix} \quad \mathbf{B}_2^{60,\text{lon}} = \begin{bmatrix} 2.4211 & -0.0967 \\ -7.0297 & -0.0885 \\ -0.4991 & 6.7324 \\ 0 & 0 \end{bmatrix}$$

Appendix A.2. Lateral-Directional

$$\mathbf{A}_0^{60,\text{lat}} = \begin{bmatrix} -0.0593 & 5.4404 & 9.6526 & -30.4764 \\ 0.1419 & 8.6618 & 0 & -0.8347 \\ 0 & 1 & 0 & 0.1793 \\ -0.0076 & 0.0118 & 0 & -0.1056 \end{bmatrix} \quad \mathbf{B}_0^{60,\text{lat}} = \begin{bmatrix} 0 & 0 \\ 187.0020 & 70.2918 \\ 0 & 0 \\ -4.0924 & -5.2289 \end{bmatrix}$$

$$\mathbf{A}_1^{60,\text{lat}} = \begin{bmatrix} 0.0005 & 0.2019 & 0.0056 & 0.0407 \\ 0.3087 & 0.8971 & 0 & -0.2831 \\ 0 & 0 & 0 & 0.0065 \\ -0.0082 & -0.0545 & 0 & 0.0093 \end{bmatrix} \quad \mathbf{B}_1^{60,\text{lat}} = \begin{bmatrix} 0 & 0 \\ 4.5751 & 3.5632 \\ 0 & 0 \\ 0.2347 & 3.2797 \end{bmatrix} \tag{A2}$$

$$\mathbf{A}_2^{60,\text{lat}} = \begin{bmatrix} 0.0016 & 0.2411 & 0 & -0.0905 \\ -0.2998 & 0.0154 & 0 & 0.1552 \\ 0 & 0 & 0 & 0 \\ 0.0114 & 0.0009 & 0 & -0.0748 \end{bmatrix} \quad \mathbf{B}_2^{60,\text{lat}} = \begin{bmatrix} 5.7266 & 0.0076 \\ 12.9022 & 4.1542 \\ 0 & 0 \\ -0.5449 & -6.1028 \end{bmatrix}$$

Appendix B

The parametric reference-model matrices expressed in the affine form.

Appendix B.1. Longitudinal

$$\mathbf{A}_{m0_\theta} = \begin{bmatrix} -\tau_u & 0 & 0 & -\tau_u \\ 0 & -\tau_w & 0 & 0 \\ 0 & 0 & -6.96 & -19.05 \\ 0 & 0 & 1 & 0 \end{bmatrix} \quad \mathbf{B}_{m0_\theta} = \begin{bmatrix} 0 & 0 \\ \tau_w & 0 \\ 0 & -19.05 \\ 0 & 0 \end{bmatrix}$$

$$\mathbf{A}_{m1_\theta} = \begin{bmatrix} 0 & 0 & 0 & 0 \\ 0 & 0 & 0 & 0 \\ 0 & 0 & -3.1 & -6.45 \\ 0 & 0 & 0 & 0 \end{bmatrix} \quad \mathbf{B}_{m1_\theta} = \begin{bmatrix} 0 & 0 \\ 0 & 0 \\ 0 & -6.45 \\ 0 & 0 \end{bmatrix} \tag{A3}$$

where $\tau_u = 4$ and $\tau_w = 3$.

Appendix B.2. Lateral-Directional

$$\mathbf{A}_{m0_\phi} = \begin{bmatrix} -\tau_v & 0 & 0 & 0 \\ 0 & -8.61 & -29.21 & 0 \\ 0 & 1 & 0 & 0 \\ 0 & 0 & \tau_r & -\tau_r \end{bmatrix} \quad \mathbf{B}_{m0_\phi} = \begin{bmatrix} 0 & \tau_v \\ -29.21 & 0 \\ 0 & 0 \\ 0 & 0 \end{bmatrix}$$
$$\mathbf{A}_{m1_\phi} = \begin{bmatrix} 0 & 0 & 0 & 0 \\ 0 & -3.83 & -9.85 & 0 \\ 0 & 0 & 0 & 0 \\ 0 & 0 & 0 & 0 \end{bmatrix} \quad \mathbf{B}_{m1_\phi} = \begin{bmatrix} 0 & 0 \\ -9.85 & 0 \\ 0 & 0 \\ 0 & 0 \end{bmatrix} \tag{A4}$$

where $\tau_v = 4$ and $\tau_r = 5$.

References

1. Lhachemi, H.; Saussi, D.; Zhu, G. A Structured H_∞-based Optimization Approach for Integrated Plant and Self-Scheduled Flight Control System Design. *Aerosp. Sci. Technol.* **2015**, *45*, 30–38. [CrossRef]
2. Wang, Y.; Bortoff, S. Co-Design of Nonlinear Control Systems with Bounded Control Inputs. In Proceedings of the World Congress on Intelligent Control and Automation (WCICA), Shenyang, China, 29 June–4 July 2014. [CrossRef]
3. Jiang, Y.; Wang, Y.; Bortoff, S.; Jiang, Z. Optimal Codesign of Nonlinear Control Systems Based on a Modified Policy Iteration Method. *IEEE Trans. Neural Netw. Learn. Syst.* **2015**, *26*, 409–414. [CrossRef] [PubMed]
4. Sahasrabudhe, V.; Celi, R.; Tits, A. Integrated Rotor-Flight Control System Optimization with Aeroelastic and Handling Qualities Constraints. *J. Guid. Control Dyn.* **1997**, *20*, 217. [CrossRef] [PubMed]
5. Wang, Y.; Wang, Y. A Gradient-Based Approach for Optimal Plant Controller Co-Design. In Proceedings of the American Control Conference (ACC), Chicago, IL, USA, 1–3 July 2015. [CrossRef]
6. Wang, Y.; Wang, Y.; Bortoff, S. On Extension of a Gradient-Based Co-Design Algorithm to Linear Descriptor Systems. In Proceedings of the World Congress on Intelligent Control and Automation (WCICA), Guilin, China, 12–15 June 2016.
7. Hiramoto, K.; Grigoriadis, K. Integrated Design of Structural and Control Systems with a Homotopy Like Iterative Method. In Proceedings of the American Control Conference, Portland, OR, USA, 8–10 June 2005. [CrossRef]
8. Quoc, T.; Gumussoy, S.; Michielsy, W.; Diehl, M. Combining Convex-Concave Decompositions and Linearization Approaches for solving BMIs, with application to Static Output Feedback. *IEEE Trans. Autom. Control* **2012**, *57*, 1377–1390. [CrossRef]
9. Niewoehner, R.; Kaminer, I. Integrated Aircraft-Controller Design Using Linear Matrix Inequalities. *J. Guid. Control Dyn.* **1996**, *19*, 445. [CrossRef] [PubMed]
10. Yang, G.; Lum, K. An Optimization Approach to Integrated Aircraft-Controller Design. In Proceedings of the American Control Conference (ACC), Denver, CO, USA, 4–6 June 2003. [CrossRef]
11. Berglund, E.; Kaminer, I. An Integrated Approach to Plant Optimization and Controller Design. In Proceedings of the IFAC Symposium on Robust Control Design, Budapest, Hungary, 25–27 June 1997; pp. 213–218.
12. Kaminer, I.; Howard, R.; Buttrill, C.S. Development of Closed-Loop Tail-Sizing Criteria for a High Speed Civil Transport. *AIAA J. Aircr.* **1997**, *34*, 658. [CrossRef] [PubMed]
13. Anonymous. *Aeronautical Design Standard, Performance Specification, Handling Qualities Requirements for Military Rotorcraft*; Ads-33e-prf; U.S. Army Aviation and Missile Command, Aviation Engineering Directorate: Redstone Arsenal, AL, USA, 2000.
14. Orhan, E.; Tekinalp, O. Integrated Plant and Controller Design Optimization: An LQR Based Approach for VTOL Air Vehicle Design Problem. In Proceedings of the Ankara International Aerospace Conference (AIAC), Ankara, Turkey, 17–19 September 2025.
15. Orhan, E.H.; Tekinalp, O. Integrated Plant and Controller Design: An H_∞ Based Solution for VTOL Air Vehicle Sizing Problem. In Proceedings of the VFS Forum 82, West Palm Beach, FL, USA, 5–7 May 2026.
16. Okcu, I. A Comparison of Model Following Control Systems for Helicopter Flight Control Near Hover. Master's Thesis, Middle East Technical University, Ankara, Turkey, 2015.
17. Yu, H.; Duan, G. *LMIs in Control Systems—Analysis, Design and Applications*; CRC Press: Boca Raton, FL, USA, 2013.
18. Hilbert, K. *A Mathematical Model of the UH-60 Helicopter*; Nasa-tm-85890; NASA: Moffett Field, CA, USA, 1984.
19. Talbot, P.; Tinling, B.; Decker, W.; Chen, R. *A Mathematical Model of a Single Main Rotor Helicopter for Piloted Simulation*; Nasa tm-84281; NASA: Moffett Field, CA, USA, 1982.
20. Niemiec, R.; Gandhi, F.; Lopez, M.J.S.; Tischler, M. System Identification and Handling Qualities Predictions of an eVTOL Urban Air Mobility Aircraft Using Modern Flight Control Methods. In Proceedings of the Vertical Flight Society 76th Annual Forum, Virtual, 5–8 October 2020.

21. Key, D.L.; Blanken, C.L. *Background Information and User's Guide for Handling Qualities Requirements for Military Rotorcraft*; Rdmr-ad-16-01; Ames Research Center: Moffett Field, CA, USA, 2015.
22. Antonioli, J.; Taghizad, A.; Rakotomamonjy, T.; Ouladsine, M. Towards the development of a methodology for designing helicopter flight control laws by integrating handling qualities requirements from the first stage of tuning. In Proceedings of the 40th European Rotorcraft Forum, Southampton, UK, 2–5 September 2014.
23. Niewoehner, R.J. Plant/Controller Optimization by Convex Methods. Ph.D. Thesis, Naval Postgraduate School, Monterey, CA, USA, 1994.
24. Lofberg, J. YALMIP: A Toolbox for Modeling and Optimization in MATLAB. In Proceedings of the IEEE International Conference on Robotics and Automation, Taipei, Taiwan, 2–4 September 2004. [CrossRef]

Disclaimer/Publisher's Note: The statements, opinions and data contained in all publications are solely those of the individual author(s) and contributor(s) and not of MDPI and/or the editor(s). MDPI and/or the editor(s) disclaim responsibility for any injury to people or property resulting from any ideas, methods, instructions or products referred to in the content.